Atom-Trap BECs

A new laboratory for studying superfluidity, quantum fluctuations, and other quantum phenomena

Eddy M. E. Timmermans

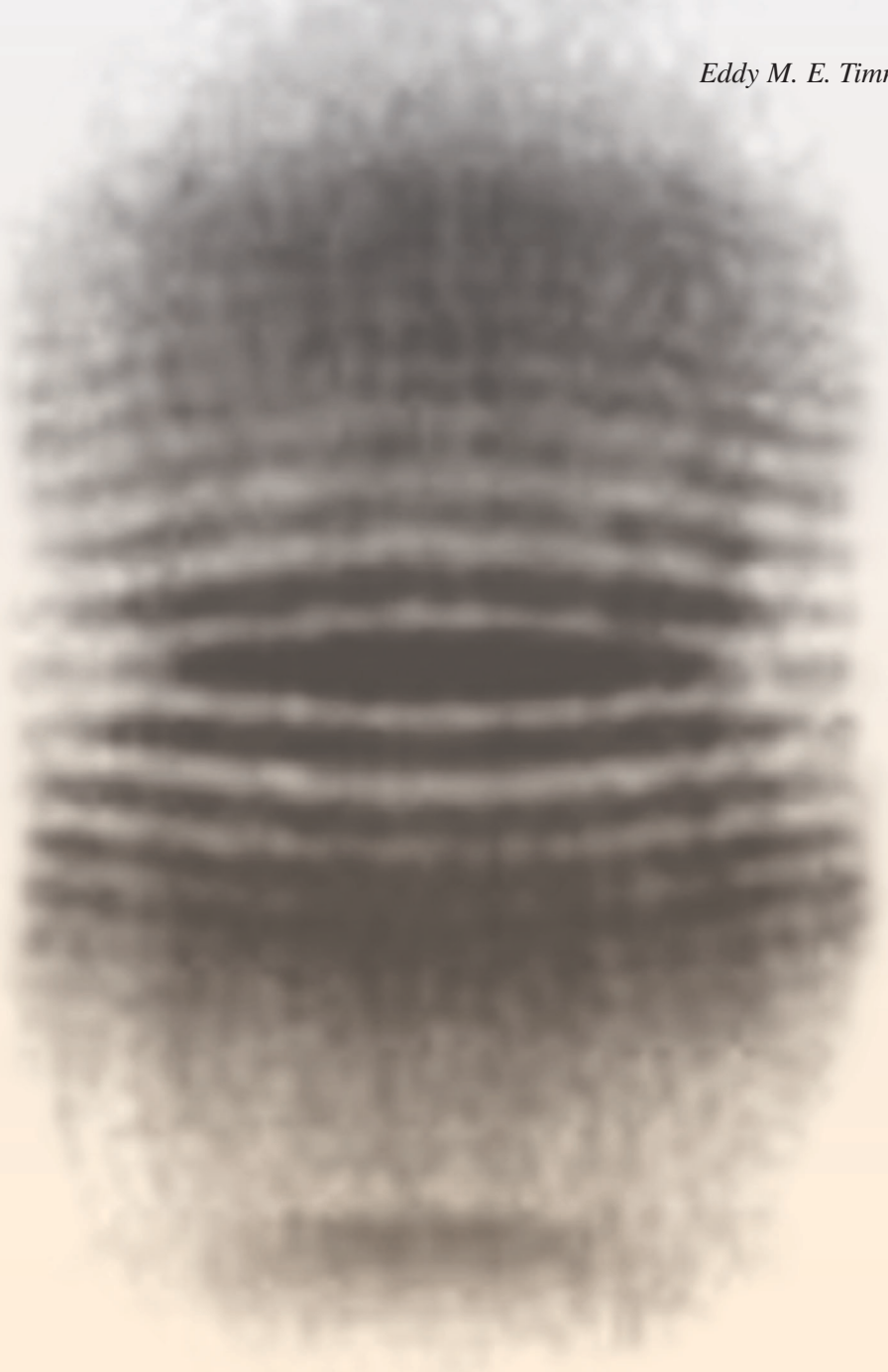

In October 2001, the field of ultracold-atom physics was honored with the Nobel Prize in physics. It was awarded to Carl Wieman, Eric Cornell, and Wolfgang Ketterle for the creation and study of dilute-gas Bose-Einstein condensates (BECs). Never before had the BEC phase transition, predicted by Einstein more than 70 years earlier, been observed in such a clear and unambiguous realization. By confining neutral atoms in a tiny magnetic trap and cooling them to temperatures only nanokelvins above absolute zero, the Nobel laureates and their colleagues had slowed the atoms down to the point at which the individual wave functions begin to overlap and many thousands of atoms suddenly occupy exactly the same single-particle quantum state. Coaxing bosonic atoms (atoms with integer spin) to condense into this coherent quantum state had been the "holy grail" of the cold-atom physics community for almost two decades. The quest had led to the development of extraordinarily clever trapping and cooling techniques, including Zeeman slowing, magneto-optical trapping, evaporative cooling, and time-orbital potential trapping. The achievement of the first atomic BECs in the summer of 1995 has led to a remarkable sequence of advances that continues unabated.

At first, this article first provides a historical perspective on atom-trap BECs and then focuses on the exciting experiments that are driving the field of cold-atom physics. Our historical overview stresses the long-range coherent properties of BECs and the role BEC physics has played in the explication of superfluidity in liquid helium. In discussing current work, we have selected a line of research and a series of experiments that illustrate the enormous flexibility of the new atom-trap BEC technologies. These experiments were carried out at the Massachusetts Institute of Technology (MIT), Yale University, and Max Planck Institute of Physics in Munich, Germany. Their achievements suggest intriguing prospects for future work in ultracold atomic physics in general and at Los Alamos in particular. In fact, several Los Alamos scientists have already contributed to the development of this field on an individual basis, and we briefly mention those in the concluding section.

The opening figure, produced by Ketterle's group at MIT, is taken from the paper (Andrews et al. 1997) that provides the starting point for our discussion of the new avenues introduced by these advances. The figure is a direct optical image of two ballistically expanding BECs showing a spatial interference pattern on a macroscopic scale. This pattern is a stunning confirmation that the phase coherence in atom-trap BECs is as complete as in optical lasers, and therefore these condensates can be manipulated and used as atomic lasers, that is, as coherent sources of atomic-matter waves. This is a unique prospect for phase-coherent matter.

After we introduce and resolve an intriguing puzzle regarding the origin of the interference pattern, we turn to a BEC experiment by the group of Mark Kasevich at Yale. This experiment is interesting from a theoretical point of view because the BECs display both laserlike and superfluid aspects of long-range phase coherence. The former is usually reserved for a nonequilibrium system of noninteracting photons, whereas the latter is usually reserved for an equilibrium or near-equilibrium fluid of strongly interacting helium atoms. Specifically, adjacent weakly linked BECs display laserlike spatial interference in a manner that implies Josephson-junction-like phase dynamics between the BECs (Orzel et al. 2001).

The purpose of the Yale experiment was not to probe coherent behavior but to induce and observe quantum fluctuations in the conjugate variables of long-range phase versus localized atom number. The group loaded the BECs into an optical lattice in which the potential barriers separating the lattice wells serve as junctions. By gradually freezing out the motion of the bosons through the junctions and observing the subsequent loss of phase coherence, the scientists were able to infer an increased certainty in the number of atoms in each well, that is, the formation of number-squeezed states. A few months later, the group of Theodore Hänsch in Munich, Germany (Greiner et al. 2002), conducted a beautiful experiment that took this process to its limit. They observed the sudden disappearance of all phase coherence in a BEC trapped in an optical-lattice potential, a direct demonstration of the Mott-insulator phase transition in which a partly coherent state becomes an all-localized state and the tunneling between wells completely stops. This transition is somewhat analogous to the well-known Mott transition from a conducting phase to an insulating phase of electrons in a crystal lattice.

The success of these experiments is due in part to the fact that dilute-gas BECs, with their long coherence lengths and slow evolution times, are readily manipulated and observed with high-precision atomic and optical technologies. Atom-trap BECs have become a remarkably flexible and transparent system for exploring complex many-body phenomena.

In introducing a theoretical view of these developments, we use a "pedestrian" approach to the condensate description, drawing the comparison to single-particle quantum mechanics wherever possible. This approach will make some of the more subtle points of many-body condensate physics accessible to the nonspecialist. We end with an assessment of the atom-trap BEC system for investigating fundamental issues in many-body physics.

Atom-Trap BECs—A Realization of Einstein's Condensate

Einstein was the first to understand the quantum concept of particle indistinguishability and to realize some of its far-reaching implications. He made the following prediction: When a gas of noninteracting bosons, or particles with integer spin, is cooled below a critical temperature, a significant fraction of the particles will suddenly find themselves in the same lowest-energy single-particle state. (This is an example of a many-body system that is "quantum degenerate," a term signifying that the system's behavior is dominated by quantum statistics—that is, the statistics of indistinguishable particles, either Bose statistics for particles with integer spin or Fermi statistics for particles with half-integer spin—as opposed to the Boltzmann statistics of classical systems.) In the limit of zero temperature, all the noninteracting bosons would occupy exactly that same ground state yielding a many-body state that we now call a BEC.

Similarly, in the ground state of a dilute gas of bosons, almost all particles find themselves in the same single-particle quantum state. Much attention has been devoted over the years to the study of such dilute-gas BECs because they are believed to provide a

model for studying superfluidity in a more direct way. The term "superfluidity" denotes a host of low-temperature fluid phenomena such as inviscid, or dissipationless, flow and quantized vortices, all of which contradict our intuition for classical fluid behavior. Interestingly, all condensed-matter superfluids such as helium-4, its fermion cousin helium-3, and the superconductors consist of strongly interacting particles and do not resemble dilute-gas BECs in most of their particulars. However, we believe that their superfluid nature arises from the property of long-range phase coherence, which they share with the dilute-gas BECs. The concept of long-range phase coherence will be discussed later. For now, simply stated, it implies the existence of a complex-valued, single-particle-like wave that characterizes the entire many-body system.

In the case of a dilute BEC, the single-particle-like quantum wave (a wave function that depends on the position of a single particle) can be identified with the wave function of the single-particle state that is occupied, on average, by more than one boson and is also known as the multiply occupied single-particle state.[1] Because almost all particles occupy that single-particle state at zero temperature, the dilute BEC exhibits almost complete coherence. The dilute BEC is then the simplest superfluid system. In contrast, the precise description of the quantum wave coherence of a strongly interacting superfluid is not straightforward. Although it is tempting, for instance, to associate the fraction of the fluid that is superfluid (and can flow without dissipation) with the fraction of the atoms that occupy the lowest-energy single-particle state, that assumption turns out to be wrong. At zero temperature, the helium-3 fluid is all superfluid, whereas only 10 percent of the atoms occupy the zero-momentum state.

Questions regarding the strong interaction effects and the role of quantum fluctuations in reducing the phase coherence and superfluid fraction remain of interest. Against this backdrop, it may be worth noting that the optical-lattice BEC experiments described below give unprecedented control of such quantum fluctuations.

The current atom-trap BECs are dilute in a sense that we will specify shortly. Their experimental achievement represented the first unambiguous realization of dilute BECs. They are made from neutral alkali atoms (sodium, rubidium, lithium, and more recently, hydrogen) that are trapped and cooled with a combination of optical and magnetic fields. (See "Experiments on Cold Trapped Atoms" on page 168 for a description of trapping and cooling processes.) The alkali atoms chosen consist of an even number of fermions (protons, neutrons, and electrons) giving a total spin that has an integer value. These "composite" bosons exhibit the same type of "gregarious" behavior that Einstein predicted for noncomposite bosons. Indeed, the experimenters knew that a BEC had formed when they saw evidence for a sudden increase in the number of atoms occupying the same single-particle ground state at the center of the trap (see Figure 1). This "condensation" is quite different from the familiar liquid-vapor phase transition seen in water, for example. The particle wave functions overlap perfectly, and the behavior of this degenerate Bose-Einstein gas, or condensate, becomes exquisitely sensitive to the interparticle interactions even if the system is dilute. The spatial extent of the multiply occupied single-particle wave function is determined by the competition of the effective interparticle repulsion and the trapping potential that confines the atoms. In present-day experiments, the size of the BEC can be as large as one-tenth of a millimeter. In other words, the multiply occupied single-atom wave function describing the BEC is macroscopic.

Although Bose-Einstein condensation had never been directly observed before 1995, this phase transition served as a textbook example in statistical mechanics (Huang 1987) because it is one of the few phase transitions that can be described analytically. As Einstein himself stressed (Pais 1979), this remarkable transition follows solely from the quantum-mechanical concept of particle indistinguishability, unlike the usual phase

[1] A multiply occupied single-particle state is mathematically expressed in Equation (1) of this article.

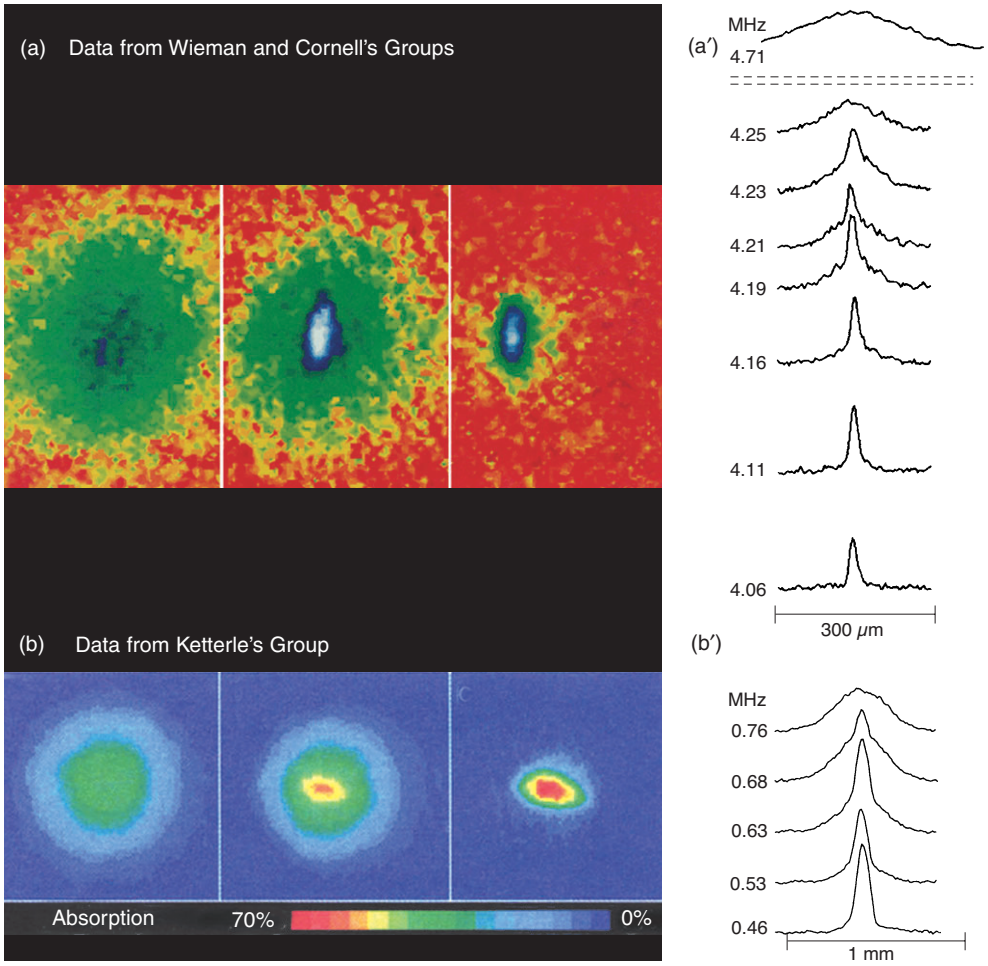

Figure 1. The First Atom-Trap BECs

Some of the first signatures of Bose-Einstein condensation were obtained in a dilute gas of trapped rubidium atoms in the groups of Wieman and Cornell. Shown in (a) are the shadow (absorption) images of the density profile of the trapped atoms and in (a′) the cross sections of the local density. Both data sequences were obtained with varying values of the cutoff energy used in the evaporative cooling, the final stage in cooling the trapped atoms. In evaporative cooling, atoms of energy above the cutoff, indicated in megahertz, were removed from the trap. As the cutoff energy decreases, the final temperature to which the system equilibrates is lowered. Below a critical value, a sharp peak appears in the density profile, a signal that Bose-Einstein condensation has occurred. As the gas was contained in an asymmetric (cigar-shaped) trap, the shape observed in (a) provides an independent signature. The leftmost frame shows a spherically symmetric thermal cloud; the middle frame shows an asymmetric density spike corresponding to the condensate surrounded by a thermal cloud; and the rightmost frame shows the final density spike in which most of the atoms have Bose-condensed. (b) These shadow images from Ketterle's group show a BEC in sodium. The number of trapped atoms is greater than that in (a) by about a factor of 100. The density of the condensate grows with decreasing temperature from left to right. (b′) These density plots show cuts through an atomic cloud as the condensate develops. Note that the spatial extent of the condensate is about 0.1 mm. The size reflects the macroscopic nature of the system. It increases with the scattering length defined in the text.

[Figures 1(a) and 1(a′) are reprinted with permission from Anderson et al. *Science* 269, page 199. Copyright 1995 American Association for the Advancement of Science. Figures 1(b) and 1(b′) are reproduced with permission from the American Physical Society.]

transitions, which result from a competition between interactions and entropy (disorder).

The neutral atom-trap systems are extremely dilute. Like billiard balls, they feel each other's presence only when they are separated by a distance equal to or less than a particular length. This length, known as the scattering length a, takes on different values for different atomic species—or even for the same species in different atomic states—but for most of the trapped neutral alkali atoms, its value is positive (reflecting an effectively repulsive force between the particles), and it tends to be about 1 nanometer. We characterize the "diluteness" of the gas by visualizing the atoms as hard spheres of radius a and computing the fraction of the total volume occupied by the spheres, $(4\pi/3)na^3$, also called the "packing fraction." In the current atom-trap BECs, the packing fraction ranges from one part in a million to one part in a billion.

At that diluteness, almost all atoms are phase coherent in the zero-temperature Bose-condensed state, somewhat in the manner that the photons produced through stimulated emission into a single mode of an optical-laser cavity are phase coherent. That is, all particles behave according to the same coherent wave function, and the particles can exhibit macroscopic interference. Contrary to the optical-laser system, the BECs consist of mutually interacting particles that are conserved (that is, the total number of atoms remains constant) and that can relax to an equilibrium state, in which case the long-range phase coherence gives rise to superfluid behavior. Indeed, in the last three years,

experiments have definitively shown that the atom-trap BECs exhibit the defining behavior of a superfluid such as sustained superflow (or dissipationless flow), zero resistance to an object moving through the condensate, and quantized vortices.

Most BEC experiments are carried out with no more than a hundred thousand to a few million atoms. The difficulties encountered in increasing the particle number currently limits the prospects for practical applications somewhat. On the other hand, the atom-trap BEC technology has become fairly routine—more than 20 experimental groups have achieved BECs by now. The extraordinary flexibilities offered by the available atomic, molecular, and optical technologies, as well as by the imaging techniques, provide the BECs with advantages that are unique in low-temperature physics.

Aspects of BEC Dynamics

We will explore a bit further the two quantum concepts that are central in understanding BECs and the sense in which superfluid behavior of the BECs represents the behavior seen or inferred in liquid helium and other systems, including nuclei, subnuclear systems produced in accelerators, and neutron stars. Those two central concepts are particle indistinguishability and coherent wave behavior.

Particle Indistinguishability. It was Einstein who realized that the statistics Bose devised to understand the Planck spectrum of black-body radiation involved counting the number of ways in which particles (in that case, photons) can be distributed over single-particle states (called "subcells" in Einstein's thermodynamic treatment). The Bose counting presumed the particles to have a distinctly nonclassical quality. Whereas the trajectories of classical particles can always be followed so that the particles can be distinguished from each other, Bose counting assumed particles to be fundamentally indistinguishable. Einstein extended the counting technique for photons, whose particle number is not conserved, to a gas of conserved noninteracting particles, and he showed that the indistinguishability implies a sudden increase in the number of particles occupying the specific subcell/single-particle state of lowest energy: the BEC phase transition.

Coherent Wave Behavior. A BEC's coherent wave behavior follows directly from the time evolution of the multiply occupied single-particle state. In quantum mechanics, the one-particle system evolves according to Schrödinger's wave equation. As a consequence, the single-particle system can exhibit the type of interference seen in Young's classic double-slit experiment, which proved that light was a wave phenomenon (see the box "The Double-Slit Experiment"). In the quantum interpretation, light and atoms exhibit both particle and wave behavior, and the interference results from the uncertainty in knowing which of two possible trajectories the particle or the photon followed in reaching the detector. (Put another way, the particle can simultaneously follow two different paths to reach the screen; that is, it can exist in a superposition of probability amplitudes A_1 and A_2, one for each path. The probability of finding the particle at the detector is given by the square of the amplitude $|A_1 + A_2|^2$, which exhibits interference that is due to the $A_1A_2^* + A_1^*A_2$ contribution.) Depending on the location at which the particles hit the detector, the probability amplitudes for each path add up constructively or destructively, respectively increasing or decreasing the probability.

As explained in the box, the observation of an interference pattern, even with light, can represent an experimental challenge. Many particles (or photons) must pass through the slits for the pattern to be seen, and if the particles (photons) occupy different single-particle states, the interference washes out, and the probability becomes a single blob without the spatial oscillations that signal interference. In the BEC case, as in an optical-

The Double-Slit Experiment—A Quantitative Measure of Coherence

In 1802, Young devised and performed the double-slit experiment, which disproved Newton's particle theory of light and established unequivocally that light is a wave phenomenon. In that experiment, two holes punched in a screen allowed incident light to pass through. The light intensity reaching a second screen located behind the first was then recorded, and under the right conditions, it was possible to observe interference fringes (an intensity pattern that oscillates in space), giving unmistakable proof of the wave nature of light.

To understand the origin of the interference fringes, we imagine the light to be perfectly monochromatic (characterized by a single wavelength or frequency) and to be emitted in a direction perpendicular to the screens from a point source an infinite distance away (see Figure A). In that case, the incident light consists of plane waves with wave fronts parallel to the screen. The light reaching a specific position on the second screen has traveled in a straight line from either hole, and the difference in distance traveled determines the difference in phase of both light rays reaching the screen. If the difference in distance traveled by each ray is equal to an integer number of wavelengths, the waves originating from each hole are in phase, which means that their instantaneous electric-field vectors point in the same direction. The total electric field, which is the vector sum of both fields, then has a magnitude equal to the sum of the magnitudes. In contrast, if the difference in distance is equal to an odd number of half-wavelengths, the waves are out of phase, meaning that the electric-field vectors of the rays that passed through the different slits point in opposite directions and that the magnitude of their vector sum is less than that of the light from a single hole. In fact, they can completely cancel each other out, giving a vanishing intensity. In the first case, the waves are said to add up constructively, and the intensity, which is proportional to the square of the magnitude of the total electric-field vector, appears bright; in the latter case, the waves add up destructively, and the intensity appears dim. Varying the position on the second screen causes the difference in distance from both holes to vary and the intensity to go through a series of maxima and minima, corresponding to, respectively, constructive and destructive interference.

In a realistic two-slit experiment, the incident waves are not perfectly monochromatic, and the source of light is not a perfect point source. Whether the interference pattern can be distinguished in the recorded intensity actually depends on the details of the experiment, such as the distance between the slits. Loosely speaking, optical coherence refers to the ability of the light to exhibit such interference. Mathematically, the contrast is specified by measurements of the highest (I_{max}) and lowest (I_{min}) intensities. The visibility of the fringes, defined as the ratio $(I_{max} - I_{min})/(I_{max} + I_{min})$, provides a measure of light coherence. For laser light, the slits can be as far apart as the width of the laser beam and still produce an interference pattern with a visibility near unity. In the quantum description of the laser, nearly all photons are said to be in the same state. In contrast, thermal light contains photons in different states, each of which would give a different interference pattern with interference fringes at different positions. The recorded pattern is a sum of all the interference patterns, and the fringes at different positions can wash each other out.

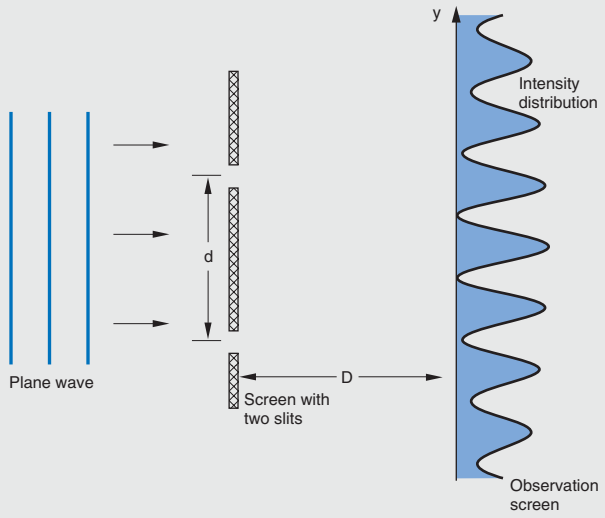

Figure A. Diagram of Double-Slit Experiment
A plane wave incident on the first screen passes through the two slits and is stopped by the second screen. The light intensity at a specific position on the second screen depends on the difference in the path lengths traveled by the light waves emanating from the two slits to that position. If the path length difference is equal to an odd number of half wavelengths, the spot appears dim (low intensity); if it is equal to an integer number of wavelengths, the spot appears bright (high intensity). The path length difference varies along the straight line shown in the plane of the second screen. Along this line, the intensity passes through positions of constructive and destructive interference, giving an oscillatory intensity variation, called interference fringes.

laser system, most particles occupy the same state so that the many-particle system exhibits the interference pattern of the single-particle system. We call this property "coherent wave behavior." As mentioned previously, it is the essential property that the weakly interacting BEC has in common with the strongly interacting superfluids such as helium.

Classical or Mean-Field Description of BEC Dynamics. Current atom-trap BECs have packing fractions of about one part in a million to one part in a billion. At that diluteness, almost all the neutral atoms of a near-equilibrium system at near zero temperature occupy the same single-particle state. The many-body system can therefore be approximated by an N-particle wave function consisting of a product of single-particle wave functions:

$$\Psi\left(\mathbf{r}_1,\mathbf{r}_2,\ldots,\mathbf{r}_N;t\right) \approx \chi\left(\mathbf{r}_1;t\right)\chi\left(\mathbf{r}_2;t\right)\ldots\chi\left(\mathbf{r}_N;t\right) , \tag{1}$$

where the single-particle χ-function is a complex-valued quantity:

$$\chi\left(\mathbf{r};t\right) = \left|\chi\left(\mathbf{r};t\right)\right| \exp\left(i\theta\left(\mathbf{r};t\right)\right) . \tag{2}$$

In 1927, shortly after the discovery of quantum mechanics, Erwin Madelung pointed out that the behavior of the single-particle wave function was analogous to that of a fluid in which $|\chi(\mathbf{r};t)|^2$ plays the role of the single-particle density and $(\hbar/m)\nabla\theta$ is associated with a velocity. Similarly, in BEC physics, where the single-particle wave function is multiply occupied, the phase of the single-particle wave function, θ, plays a crucial role in the theory as the single phase that gives rise to all the coherent wave phenomena discussed below. In particular, its gradient describes the velocity associated with the dissipationless flow observed in superfluid systems.

The product state in Equation (1) is a special case of the Hartree-Fock Ansatz for the many-body wave function of identical particles, and it evolves according to a Hartree-Fock equation of motion. If the boson particles of mass m experience an external trapping potential V, so that the potential energy of a single boson at position $\mathbf{r}$ is $V(\mathbf{r})$, and if the bosons interact with each other through an interaction potential v, so that a pair of bosons located respectively at $\mathbf{r}$ and $\mathbf{r}'$ experience an additional energy $v(\mathbf{r}-\mathbf{r}')$, then the Hartree-Fock equation takes on the following form:

$$i\hbar\frac{\partial\chi}{\partial t} = \left[-\frac{\hbar^2\nabla^2}{2m} + V\left(\mathbf{r}\right)\right]\chi + \left[N-1\right]\int d^3\mathbf{r}'\, v\left(\mathbf{r}-\mathbf{r}'\right)\left|\chi\left(\mathbf{r}';t\right)\right|^2 . \tag{3}$$

Because the interaction between neutral atoms in a BEC has a much shorter range than the length scales on which the atom-trap BECs vary, we can approximate the interparticle potential by an effective contact interaction, $v(\mathbf{r}-\mathbf{r}') \rightarrow \lambda\delta(\mathbf{r}-\mathbf{r}')$, where the interaction strength λ is proportional to the scattering length a: $\lambda = (4\pi\hbar^2/m)a$. In addition, the number of particles is large enough to allow approximating $(N-1)$ by N. We then introduce the condensate field Φ as $\Phi = N^{1/2}\chi$ so that $|\Phi|^2$ represents the

particle density, as it does in the single-particle case. With these quantities, the Hartree equation for atom-trap BECs takes on the form of the celebrated Gross-Pitaevski equation:

$$i\hbar \frac{\partial}{\partial t} \Phi = \left[-\frac{\hbar^2 \nabla^2}{2m} + V + \lambda \left| \Phi^2 \right| \right] \Phi \ . \tag{4}$$

This equation, first derived by Pitaevski to treat superfluid vortices in a full quantum description, has been very popular in many fields of physics (and even biology). In spite of its simplicity, it has solutions that exhibit crucial nonlinear physics phenomena such as solitary waves, self-focusing, and self-trapping. As a result, the atom-trap BECs can also be regarded as new laboratories for studying nonlinear dynamics.

Describing the physics of BECs by means of the Gross-Pitaevski equation—Equation (4)—is known as "making the mean-field approximation" or "working in the classical approximation." The term "classical" may appear out of place because Equation (4) implies that matter has wavelike behavior, and it implicitly contains the Planck constant. Nevertheless, this equation also follows from the Lagrange equations of the corresponding classical field theory without any quantization condition. The Gross-Pitaevski equation gives a classical description of BECs in the same sense that Maxwell's equations provide a classical description of photon dynamics. Perhaps most significantly, the Gross-Pitaevski equation provides the simplest possible description of a superfluid system, and the mean-field approximation (which for BECs is equivalent to assuming a product wave-function solution) captures many of the essential features of superfluidity. For instance, the mean-field treatment predicts a dispersion relation, or excitation spectrum, that satisfies Landau's criterion for dissipationless flow (a criterion to which we refer below). On the other hand, the Gross-Pitaevski equation is certainly not as general as the phenomenon of superfluidity. Although some long-range behavior of the helium superfluids and superconductors can be qualitatively understood when this equation is invoked, the atom-trap BECs are the only systems quantitatively described by it. Moreover, the classical description also breaks down for BECs, for example, when quantum fluctuations become important, as they do in the experiments described at the end of this article. Those experiments involve number-squeezed states and the Mott transition from a coherent, or superfluid, state to a localized state.

The Coherent Wave Nature of Superfluidity

The term "superfluidity" was first applied to a very low temperature phase of liquid helium. In 1938, Peter Kapitza and, independently, John Allan and Donald Misener discovered that below a critical temperature of 2.2 kelvins, liquid helium-4 flows without measurable dissipation through capillary tubes. It seemed that this low-temperature phase of helium-4, called He_{II}, is not governed by the usual laws of classical fluid dynamics. Subsequent experiments uncovered other counterintuitive phenomena in He_{II}, including the fountain effect, perfect heat conductivity, and persistent circular flow. Superfluidity is now the name for both this collection of phenomena and the state of matter responsible for them.

The superfluid state was so unusual and its mechanism so difficult to discern in the relatively inaccessible medium of a strongly interacting fluid that its origin remained a matter of continuing controversy for more than two decades.

Is He_{II} like a BEC? Noting that helium-3, the fermion cousin of helium-4, did not undergo a phase transition to a superfluid at similar temperatures, Fritz London suggested in 1938 that the He_{II} transition is intimately related to the boson nature of the helium-4 atoms. He further proposed that the He_{II} superfluid is, in a generalized sense, a BEC. Of course, being a strongly interacting fluid, the helium system cannot be characterized by the assumption that all atoms occupy the same single-particle state. Nevertheless, London (1938) argued that "some of the general features of the degenerate ideal Bose-Einstein gas remain intact, at least qualitatively, for this liquid." He also offered support for his thesis by calculating the BEC critical temperature for the helium density, which came out to 3.13 kelvins, remarkably close to the He_{II} transition temperature of 2.12 kelvins, measured in 1933. Although the latter agreement is largely fortuitous, London's words sound almost prophetic in retrospect: He hinted that the superflow in He_{II} was a macroscopic quantum current brought about by changes in the boundary conditions.

The Two-Fluid Description of He_{II}. Following a different track, Lev Landau and, independently, Laszlo Tisza (who was, in fact, partly motivated by London's views) proposed the two-fluid model of He_{II}, in which one component is an inviscid, irrotational superfluid that does not carry entropy. This model explained the observed effects and also correctly predicted new superfluid phenomena, such as second sound. Landau used very general assumptions to derive a criterion for superfluidity and an expression for the critical velocity above which dissipation would set in. The critical-velocity calculation, although ultimately incorrect, captured the main features of persistent flow, and a generalized form of the Landau criterion is still of great use in explaining critical velocities for superfluidity. Nicolai Nicolaevich Bogoliubov showed that a weakly interacting BEC satisfies Landau's criterion for superfluidity, but Landau continually resisted the notion that the superfluid should be associated with a BEC.

The BEC Description Revisited. Finally, Oliver Penrose (1951) and then Penrose and Lars Onsager (1956) proposed the currently accepted point of view that superfluidity is a macroscopic manifestation of coherent (hence, single-particle-like) quantum-wave behavior. This description does not contradict the two-fluid model but supersedes it in the sense that the coherent quantum-wave behavior includes phenomena, such as quantized vortices and Josephson effects, which find no explanation in the two-fluid model.

As previously mentioned, the single-particle quantum wave behavior, which is compatible with and can be described as fluidlike behavior, had been pointed out by Madelung in 1927. In his pioneering paper of 1951, Penrose derived the equation for the off-diagonal density matrix of the many-body helium fluid and then drew on Madelung's analysis of the single-particle wave function to associate the long-range part of that off-diagonal density matrix with the superfluid component of the two-fluid model. In essence, Penrose identified quantum wave coherence as the essential feature responsible for both superfluidity and the BEC-like behavior conjectured by London.

As the understanding grew that superfluidity was an outcome of quantum wave coherence, the intimate connection between superfluidity and superconductivity was realized. We now understand both phenomena to be caused by coherent quantum-wave behavior, that is, many identical particles or units whose behavior can be described by the same single-particle wave function. For a superfluid, the single unit that exhibits the quantum wave behavior is a boson particle; for a superconductor, it is a pair of fermions. Much as we regard a superfluid as a BEC of boson particles, we can regard a superconductor as a BEC of fermion pairs. Not surprisingly, therefore, the fields of

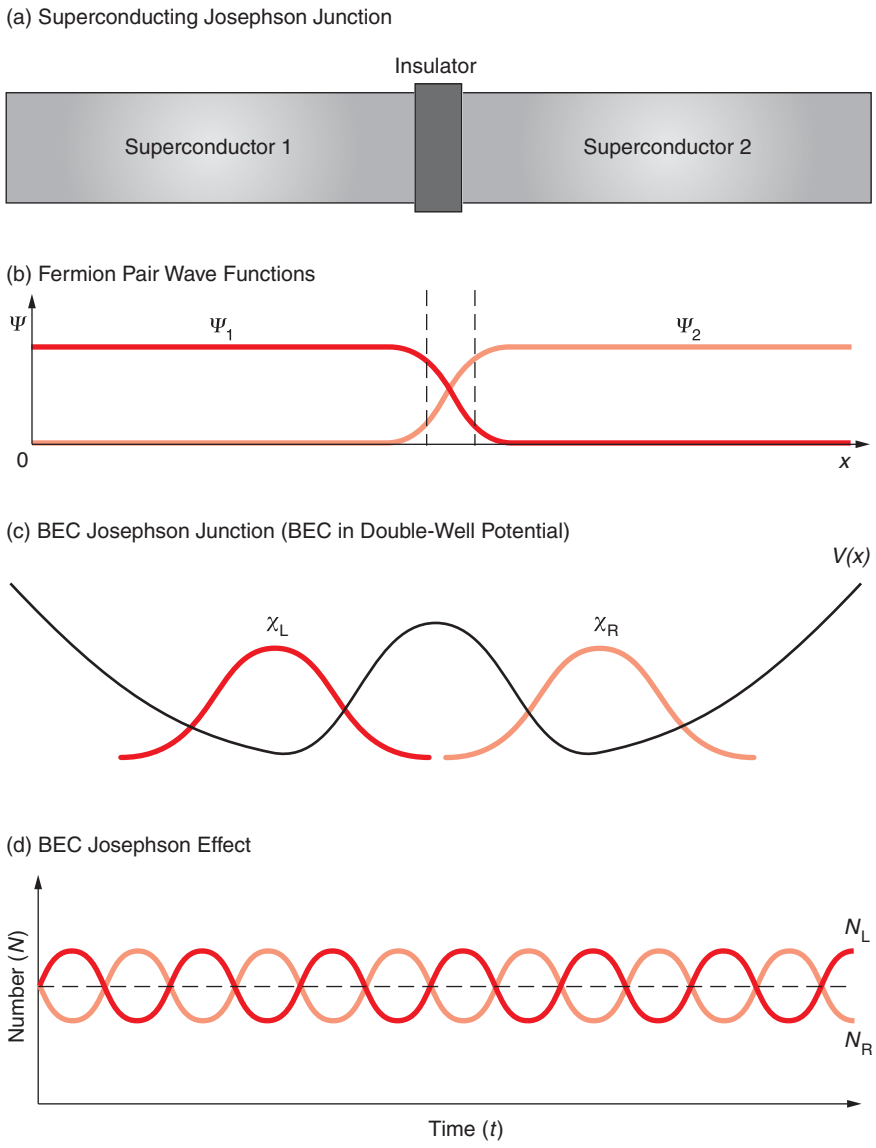

Figure 2. Josephson Junctions and the Josephson Effect for BECs
The diagrams show (a) two superconductors separated by a thin barrier and (b) the overlap of the coherent single-particle wave functions that describe each superconductor in the neighborhood of the junction. In 1962, Brian Josephson showed that, under certain conditions, quantum mechanical tunneling of electron pairs could occur through the barrier. If the two wave functions differ by a phase, a direct current of electron pairs will flow through the barrier, or junction. If a voltage is placed across the junction, the phase difference varies periodically in time, causing an alternating current to flow across the junction. (c) A neutral-atom BEC trapped in a double-well potential behaves like a superconducting Josephson junction. The potential barrier created by a laser beam acts like the insulating barrier between the superconductors. (d) The BEC junction is predicted to exhibit the Josephson effect. For instance, a sudden change in the chemical potential of one of the BECs would initiate an oscillation in the number of particles in each well. The frequency of the oscillation is determined by the difference of the chemical potentials.

superfluidity and superconductivity share a number of phenomena that stem directly from their coherent wave nature. Two of these coherent phenomena, Josephson junctions and quantized vortices, have recently been studied in atom-trap BECs and are briefly described next.

Josephson Junctions. In the 1960s, the physics of superconducting Josephson junctions provided evidence for the coherent wave nature of superconductors. The Josephson junction is a weak link, such as a thin insulator, connecting two indistinguishable superfluids or superconductors—see Figures 2(a) and 2(b). One manifestation of the Josephson "effect" is an alternating current flowing through the weak link when both sides of the junction are kept at different chemical potentials by, for instance, the introduction of a potential difference over the junction.

In an ordinary electronic circuit, the potential difference sets up a direct current (dc), which flows from the region of high chemical potential to that of low chemical potential. In contrast, in a coherent-wave superfluid system, the rate for bosons or fermion

pairs to tunnel through the potential barrier of the junction depends sinusoidally on the phase difference between the single-particle-like wave function on either side of the junction. That phase difference increases linearly with time in the presence of a potential difference, giving an alternating current that oscillates at the frequency corresponding to the chemical potential difference.

In the original condensed-matter Josephson junctions, the superfluids were superconductors. In such cases, the bosons tunneling through the junction are electron pairs, and the current is a charge current, which is easily and accurately measured. In helium superfluids, on the other hand, the weak link is difficult to make, and the observation of a weak neutral current presents a nontrivial experimental challenge, which was only recently met (Packard 1998).

The direct analogue of the Josephson junction in atom traps is an atomic BEC trapped in a double-well potential—see Figures 2(c) and 2(d). The challenge of observing the Josephson effect in this system, however, is similar to the problem encountered in observing Josephson oscillations in helium superfluids: How can one measure small-amplitude oscillations of neutral-particle populations? In the last section, we show how atom-trap BEC technology made possible a unique solution to the problem of observing Josephson phase dynamics.

Quantized Vortices. Quantized vortices are another coherent wave phenomenon unique to superfluids and superconductors. In classical fluids, vortices are long-lived flow patterns in which the particles whirl around an axis, all with the same angular momentum. In a superfluid, a superflow that similarly whirls around an axis can be set up by a characteristic variation of the coherent wave function: the phase of the wave function varies cylindrically around the vortex axis. For the wave function to be single-valued, it must return to its initial value after a full rotation around the axis; that is, its phase must have changed by 2π or by $2\pi n$, where n represents an integer number. This constraint implies that the angular momentum of superfluid vortices is quantized with allowed values equal to $n\hbar$—see Figure 3(a).

Quantized vortices in helium were observed by William Vinen and by George Rayfield and Frederick Reif, and their observations provided further support for the coherent wave behavior of the helium superfluid. In atom-trap BECs, the long-lived metastable vortex structures were created and studied in laboratories at the Joint Institute for Laboratory Astrophysics (JILA) at Boulder, Colorado, in the groups of Wieman and Cornell; at the École Normale Supérieure in Paris, in the group of Jean Dalibard; at MIT in the group of Ketterle; and at Oxford University, England, in the group of Chris Foot—see Figure 3(b). A direct measurement of the angular momentum of the vortices, by Dalibard's group, experimentally confirmed the quantization of BEC vortices. In addition, at MIT, rapid advances in BEC technology led to the creation of vortex lattices (also called Abrikosov lattices) in atom-trap BECs with up to 160 vortices and to the detailed observation at both MIT and JILA of the intricate dynamics of vortex formation and decay.

BEC Interference—A Demonstration of Wave Coherence

In optical systems, long-range phase coherence is easily demonstrated through the double-slit experiment. In fact, the sharpness of the interference fringes produced in that experiment is used as the standard measure of optical coherence. In contrast, condensed-matter systems give mostly indirect signatures of wave coherence—quantized vortices and Josephson effects—although observations and applications of temporal interference in superconductors do exist (for example, in superconducting quantum interference devices, or SQUIDS).

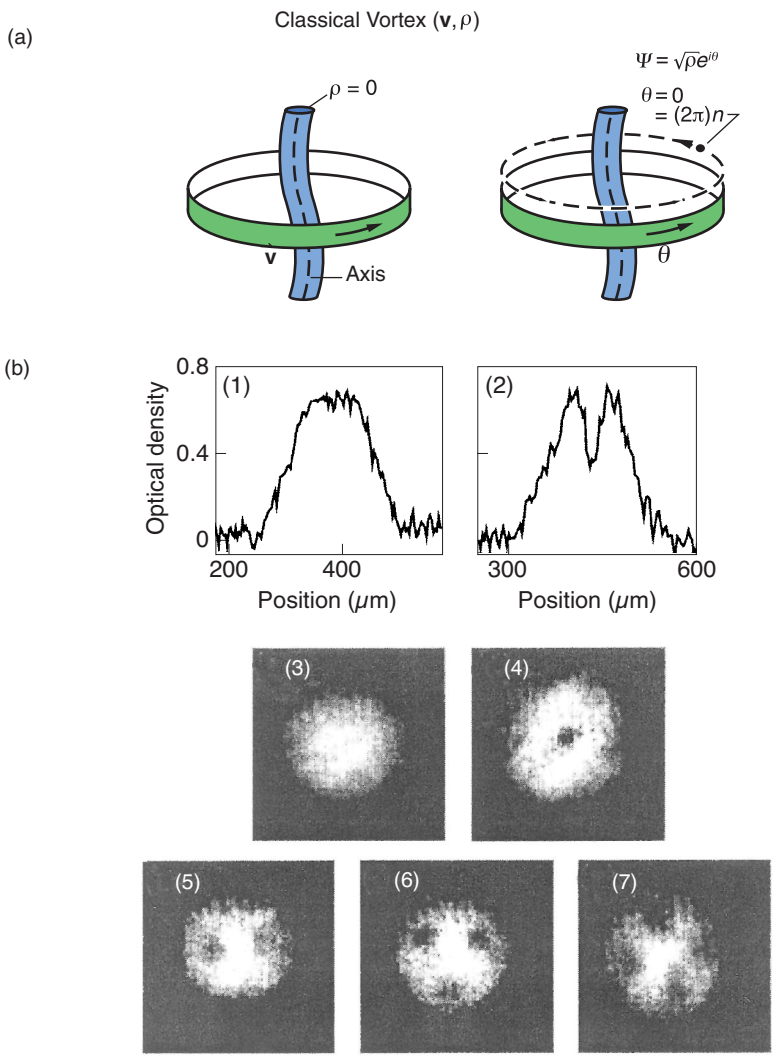

Figure 3. Quantized Vortices
(a) In a superfluid, the phase of the wave function for a vortex must increase by 2π on each revolution, which implies that the angular momentum of the vortex must be an integer multiple of $\hbar$, or $n\hbar$. (b) Several experimental groups have created and imaged quantized vortices in atom traps. The transverse absorption images (Madison et al. 2000) are of a condensate of about 10^5 rubidium-87 atoms at a temperature below 80 nK. This condensate has been stirred with a laser beam at various rotational frequencies. Above a critical rotational frequency, vortex filaments appear. Plots 1 and 2 show the variation in optical thickness along the horizontal axes of the clouds imaged in plots 3 and 4, respectively. The cloud stirred at 145 Hz (shown in plot 3) contains no vortex filament, whereas the cloud stirred at 152 Hz (shown in plot 4) contains one vortex filament. In plots 5, 6, and 7, the condensate was stirred at rotational frequencies of 169, 163, and 168 Hz, respectively.
(Reproduced with permission from *The American Physical Society*.)

Thus, when Ketterle's group at MIT observed the spectacular interference pattern shown in the opening illustration, they brought an unusual message: BECs are superfluids that can manifest their long-range phase coherence in an optical-laser-like manner of spatial interference. Michael Andrews and collaborators later (1997) argued that the interfering BEC experiment demonstrated the first atom laser (albeit in a form that, as of yet, is not necessarily useful to applications). Their demonstration suggests that the simultaneous appearance of superfluid and laserlike aspects of long-range phase coherence might one day yield particularly potent applications of BECs.

The MIT Experiment. Figure 4 outlines the experimental procedure used by the MIT group. First, an off-resonant laser beam is passed through the center of an atom trap, which effectively creates a double-well potential. The atoms are then cooled and Bose-condensed into two BECs, one on either side of the potential barrier—see Figure 5(a). Because the height of the barrier significantly exceeds the chemical potential of either BEC, the two BECs are independent.

When the trapping potential was switched off, the two BECs expanded freely and started overlapping spatially. Using two laser pulses in succession, the MIT group imaged the local density of atoms in a 100-micrometer-thick slice within the region of

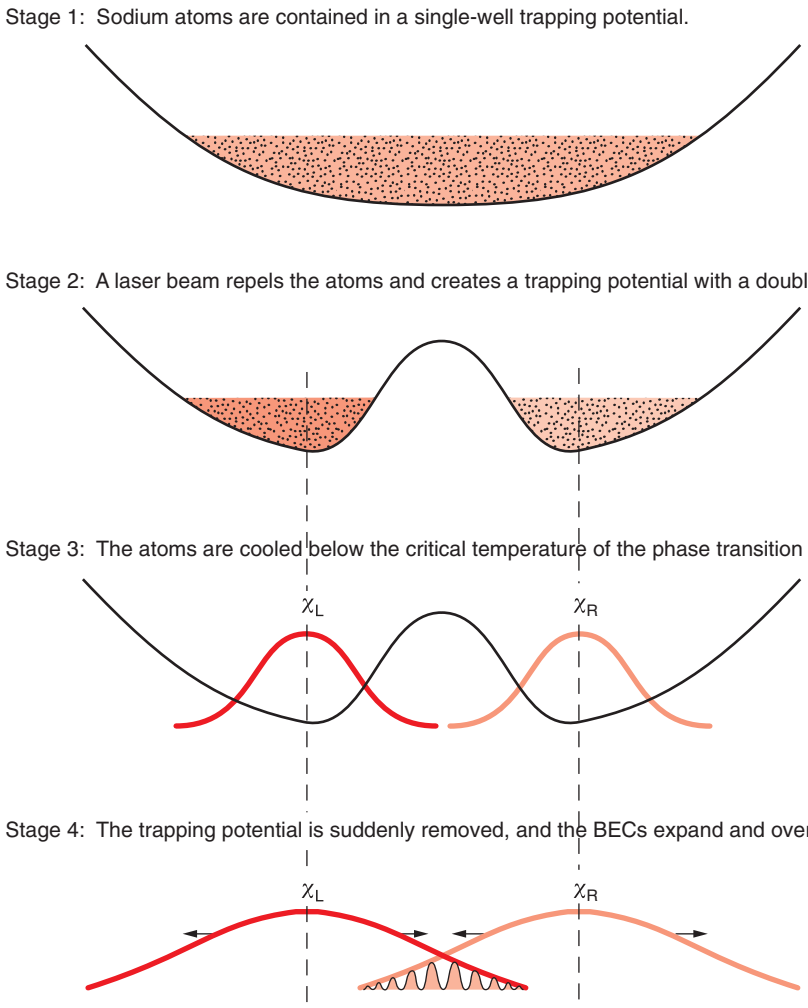

Figure 4. Procedure for Creating BEC Interference
In the BEC interference experiment conducted at MIT (Andrews et al. 1997), sodium atoms were contained in a cigar-shaped trap (stage 1). In the second stage, a laser beam focused on the center of the initial trap repelled the atoms from that region, creating an overall atomic potential that has a double-well shape. In the third stage, the atoms were cooled below the critical temperature T_C of the BEC phase transition. The height of the potential barrier separating the wells greatly exceeded the thermal energy $k_B T_C$ (where k_B denotes the Boltzmann constant) and the chemical potentials of the BECs that are formed in the left (L) and right (R) wells. (The wave functions for the two BECs are labeled χ_L and χ_R.) Under these conditions, the two BECs are independent of each other in the sense that they cannot "know" each other's phase. When the trapping potential is suddenly removed in stage 4, both BECs expand and then overlap. Images of the atomic density of the overlapping BECs show macroscopic interference fringes of high visibility.

overlap. The first laser pulse pumped the BEC atoms in the selected slice from state $|1\rangle$ to a different hyperfine state $|2\rangle$. The second laser, tuned near a resonant transition from state $|2\rangle$ to state $|3\rangle$ and pointing more or less perpendicular to the plane of the slice, imaged the density of atoms in state $|2\rangle$. The image showed a highly visible, regular pattern of clearly separated interference fringes of macroscopic size (40 micrometers)—see Figure 5(b). The visibility of the fringes (defined in the box "The Double-Slit Experiment") ranged from 20 to 40 percent. By characterizing their optics, the experimentalists inferred that the actual visibility of the density fringes ranged from 50 to 100 percent. The density fringes are defined as $(\rho_{max} - \rho_{min})/(\rho_{max} + \rho_{min})$, where ρ_{max} and ρ_{min} denote the maximum and minimum densities if observed with an ideal imaging technique. The high visibility of the observed fringes indicates that the entire many-body system behaves as a coherent wave.

What Produces the Interference Fringes? Unquestionably (by definition, in fact), macroscopic interference fringes indicate coherence in the usual optical sense. But how the observed interference fringes relate to the coherence of the expanding BECs is a matter of considerable subtlety, as will be explained. Under the experimental conditions of independent BECs, the single-particle density matrix, as we show below, does not

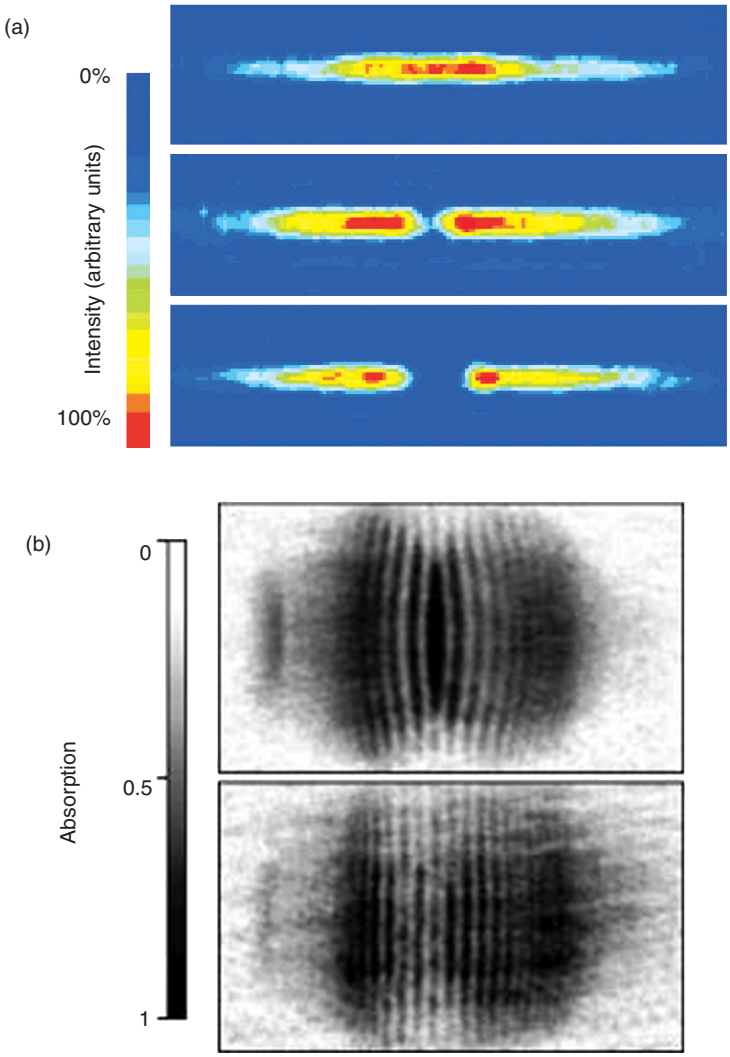

Figure 5. Sodium Atom BECs and Their Interference
(a) Phase contrast images of a single Bose condensate (upper panel) and double Bose condensates were taken in the magnetic trap of the MIT group. An argon ion laser that was focused into the center of the trap created a double-well potential. Changes from 7 to 43 mW in the power of the laser-light sheet caused the distance between the two condensates to vary. (b) The interference pattern of two expanding condensates was observed after a 40-ms time of flight for two different powers of the argon-laser-light sheet (raw-data images). The periods of the fringes were 20 and 15 μm; the laser powers were 3 and 5 mW; and the maximum absorptions were 90% and 50%, respectively, for the left and right images. The fields of view were 1.1 mm horizontally by 0.5 mm vertically. The horizontal widths were compressed fourfold, a condition that enhances the effect of the fringe curvature. For the determination of the fringe spacing, the dark central fringe on the left was excluded.

exhibit interference. Why then does the recorded image show fringes? The resolution, as we show for a special case, depends on the fact that the image does not record the single-particle density.

The Case of BECs with Definite Particle Number. As reported by Andrews et al. (1997), the potential barrier separating the two BECs was five times higher than the energy corresponding to the critical temperature for the BEC phase transition and 50 times higher than the chemical potentials of the BECs in each well. Under those conditions, the state of the double-well BEC system is indistinguishable from that of two BECs that were condensed in separate traps at an infinite distance from each other and then brought together. In principle, we can therefore know exactly how many particles occupy each of the two BECs. That is, the system is in a number state. The single-particle density of this double-well number state $\rho_{1(N)}$ does not exhibit interference, a point we now demonstrate for a simplified double-well number state with only two particles.

We call the single-atom state centered in the right well $\chi_R(\mathbf{r})$ and the single-atom state centered in the left well $\chi_L(\mathbf{r})$, where $\mathbf{r}$ denotes the center-of-mass position of the trapped atom. Thus, a two-particle number state with one atom in each well is represented by a wave function $\Psi_{(N)}$:

$$\Psi_{(N)}(\mathbf{r}_1,\mathbf{r}_2;t) = 2^{-1/2}\left[\chi_{\mathrm{L}}(\mathbf{r}_1;t)\chi_{\mathrm{R}}(\mathbf{r}_2;t) + \chi_{\mathrm{R}}(\mathbf{r}_1;t)\chi_{\mathrm{L}}(\mathbf{r}_2;t)\right] . \quad (5)$$

When the external potential is switched off, the two-particle wave function, to a close approximation, remains of the form in Equation (5), with χ_{L} and χ_{R} evolving as freely expanding single-particle wave functions that are mutually orthogonal. The corresponding single-particle density $\rho_{1(N)}$ at a given time t,

$$\begin{aligned}\rho_{1(N)}(\mathbf{r};t) &= \int d^3r_2 \left|\Psi_{(N)}(\mathbf{r},\mathbf{r}_2;t)\right|^2 \\ &= \frac{1}{2}\left[\left|\chi_{\mathrm{L}}(\mathbf{r};t)\right|^2 + \left|\chi_{\mathrm{R}}(\mathbf{r};t)\right|^2\right], \end{aligned} \quad (6)$$

is equal to an incoherent average of the densities of the individual expanding single-particle wave functions. Generally, the single-particle densities expand smoothly—a free-particle Gaussian wave function (for instance, if the χ-wave-functions start out as ground-state functions of harmonic oscillator potentials) remains Gaussian—so that $\rho_{1(N)}(\mathbf{r};t)$ does not exhibit spatial oscillations.

The Case of a Mutually Coherent State of the Double-Well System. In contrast, had a single-well system containing both particles in its center-of-mass ground state been split adiabatically, the resulting double-well system would be in a mutually coherent state. This particular mutually coherent state would be a product of single-particle wave functions of the type $2^{-1/2}[\chi_{\mathrm{L}}(\mathbf{r};t) + \exp(i\alpha)\chi_{\mathrm{R}}(\mathbf{r};t)]$, where α denotes the phase

$$\Psi_{(\mathrm{C})}(\mathbf{r}_1,\mathbf{r}_2;t) = \frac{1}{2}\left[\chi_{\mathrm{L}}(\mathbf{r}_1;t) + \exp(i\alpha)\chi_{\mathrm{R}}(\mathbf{r}_1;t)\right]\left[\chi_{\mathrm{L}}(\mathbf{r}_2;t) + \exp(i\alpha)\chi_{\mathrm{R}}(\mathbf{r}_2;t)\right], \quad (7)$$

difference that evolved between the right and left wave functions during the adiabatic splitting of the wells. This two-particle, mutually coherent wave function takes the form where the label C stands for coherent. The mean field or classical description—see Equation (1)—of the double-well BEC assumes such mutual coherence. The single-particle density of the mutually coherent, freely expanding two-particle system reads

$$\rho_{1(\mathrm{C})}(\mathbf{r};t) = \frac{1}{2}\left[\left|\chi_{\mathrm{L}}(\mathbf{r};t)\right|^2 + \left|\chi_{\mathrm{R}}(\mathbf{r};t)\right|^2 + \left(\chi_{\mathrm{L}}(\mathbf{r};t)\chi_{\mathrm{R}}^{*}(\mathbf{r};t)\exp(i\alpha) + \text{c.c.}\right)\right], \quad (8)$$

where c.c. is the complex conjugate of the previous term. Far from the potential minima of the initial wells, the amplitudes of the expanding wave functions vary slowly in space, so that we can approximate those amplitudes as $\chi_{\mathrm{R}}(\mathbf{r};t) \approx \chi \exp[i\theta_{\mathrm{R}}(\mathbf{r};t)]$ and $\chi_{\mathrm{L}}(\mathbf{r};t) \approx \chi \exp[i\theta_{\mathrm{L}}(\mathbf{r};t)]$, and the single-particle density in the far region becomes

$$\rho_{1(\mathrm{C})}(\mathbf{r};t) = \chi^2\left\{1+\cos\left[\theta_{\mathrm{R}}(\mathbf{r};t) - \theta_{\mathrm{L}}(\mathbf{r};t) + \alpha\right]\right\} . \quad (9)$$

Thus, in addition to the densities of the expanding single-particle wave functions, $\rho_{1(\mathrm{C})}(\mathbf{r};t)$ also contains an α-dependent term—namely, the interference fringes—that varies sinusoidally with the difference of the position-dependent phases of the overlapping χ_{R} and χ_{L} functions. The expression in Equation (8) is quite general; the single-particle density of an N-particle BEC distributed over two wells in a mutually coherent state takes on the form of Equation (9) in the far region.

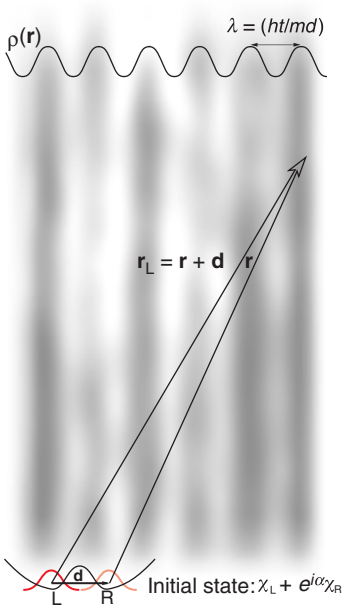

Figure 6. Geometry of Interference Fringes

The diagram shows the interference fringes in the image of two expanding BECs that were initially trapped in the right (R) and left wells (L) of a double-well potential. As defined in the text, the r-vector denotes the position relative to the center of the right well, and the d-vector denotes the relative position of the centers of both wells. The high-density regions of the interference fringes are planes oriented perpendicular to *d*. At a time *t* after releasing the BECs, the interference fringe planes are separated by a distance $\lambda = ht/(md)$. The actual positions of the fringes depend on the phase difference α of the initial BECs (if the BECs are phase coherent, $\chi = \chi_L + e^{i\alpha}\chi_R$).

Heuristic Derivation of the Interference Fringe Pattern. What is the geometry and spacing of the interference fringes that would be produced by this mutually coherent state? We offer a heuristic derivation of the phase of a freely expanding single-particle state. Classically, a particle that has traveled a distance r in a time t has a velocity $v = r/t$. In the spirit of the Madelung description, we associate the gradient of the phase θ with $mv/\hbar$, and we find $d\theta/dr = (mr/\hbar t)$, so that $\theta = (m/2\hbar)(r^2/t) + C$, where C denotes a constant, independent of $\mathbf{r}$. Now we suppose that the left and right BECs are sufficiently alike so that we can assume that their phases in the expansion evolve with the same constant C. In that case, the difference between the phases of the amplitudes χ_R and χ_L evaluated at a vector distance $\mathbf{r}$ from the center of the right well and $\mathbf{r}_L$ from the center of the left-well is

$$\theta_R - \theta_L = (m/2\hbar t)[r^2 - r_L^2\,]^2 = -\,(m/2\hbar t)[2\mathbf{d}\cdot\mathbf{r} + d^2]\ , \tag{10}$$

where the vector distance $\mathbf{d}$ separates the centers of the potential wells and $r^2 - r_L^2 = -2\mathbf{r}\cdot\mathbf{d} - d^2$ (see Figure 6). The high-density regions of the interference fringes are planes perpendicular to $\mathbf{d}$ at a regular spacing of $\lambda = \hbar t/(md)$. The measured density pattern for the density in Equation (9) is

$$\rho_{1(C)}(\mathbf{r};t) \;=\; \chi^2\Big\{\,1 \;+\; \cos\Big[\,(m/\hbar t)\,(\mathbf{r}\cdot\mathbf{d}) \;+\; (m/2\hbar t)\,d^2 \;-\; \alpha\,\Big]\Big\}\ , \tag{11}$$

and the value of α can be inferred from the positions of the interference fringe planes. A more careful derivation of the phases $\theta_{R(L)}$ gives corrections, but the above expressions are essentially correct in the regions imaged in the interfering BEC experiment. The experimental images do indeed reveal planar interference fringes, separated by a distance $\lambda = ht/(md)$.

Resolving the Origin of the Interference. The experiment clearly indicated coherence, and the image agrees with the single-particle density of the mutually coherent double-well system. However, the experimental system was prepared not in a mutually coherent state, but in a number state analogous to that described by Equation (5). In that state, given that the single-particle density $\rho_{1(N)}$ in Equation (6) does not exhibit interference, why does the recorded image show fringes like those from the coherent single-particle density in Equation (11). The resolution of this apparent puzzle lies in the fact that the image does not record the single-particle density. Instead, the experiment probes the multiparticle density. Specifically, we cannot interpret the image of the N-particle system as N independent measurements of the single-particle density. But we can assume that the measurement captures the N-body system in a "likely" configuration; that is, the observation of a particle at $\mathbf{r}_1$, another at $\mathbf{r}_2$, and so on, indicates that the state of the system corresponding to the N-particle density $\rho_N(\mathbf{r}_1, \mathbf{r}_2, \ldots, \mathbf{r}_N) = |\Psi(\mathbf{r}_1, \mathbf{r}_2, \ldots, \mathbf{r}_N)|^2$ has a relatively high probability.

We use the special case of two particles in a double-well potential to illustrate the difference in probing the N-particle rather than the single-particle density. We assume the two-particle double-well system is prepared in the number state of Equation (5). We detect the particles at a time t during a period that is short on the time scale on which the single-particle wave functions χ_L and χ_R expand. The probability that one particle is recorded at $\mathbf{r}_1$ and the other at $\mathbf{r}_2$ is proportional to the two-particle number-state density:

$$\rho_{2(N)}(\mathbf{r}_1,\mathbf{r}_2;t) \;=\; \big|\chi_L(\mathbf{r}_1;t)\big|^2\big|\chi_R(\mathbf{r}_2;t)\big|^2 \;+\; \big|\chi_L(\mathbf{r}_2;t)\big|^2\big|\chi_R(\mathbf{r}_1;t)\big|^2 \;+\; \Big[\,\chi_L(\mathbf{r}_1;t)\,\chi_R^*(\mathbf{r}_1;t)\,\chi_R(\mathbf{r}_2;t)\chi_L^*(\mathbf{r}_2;t) \;+\; \text{c.c.}\,\Big]\ . \tag{12}$$

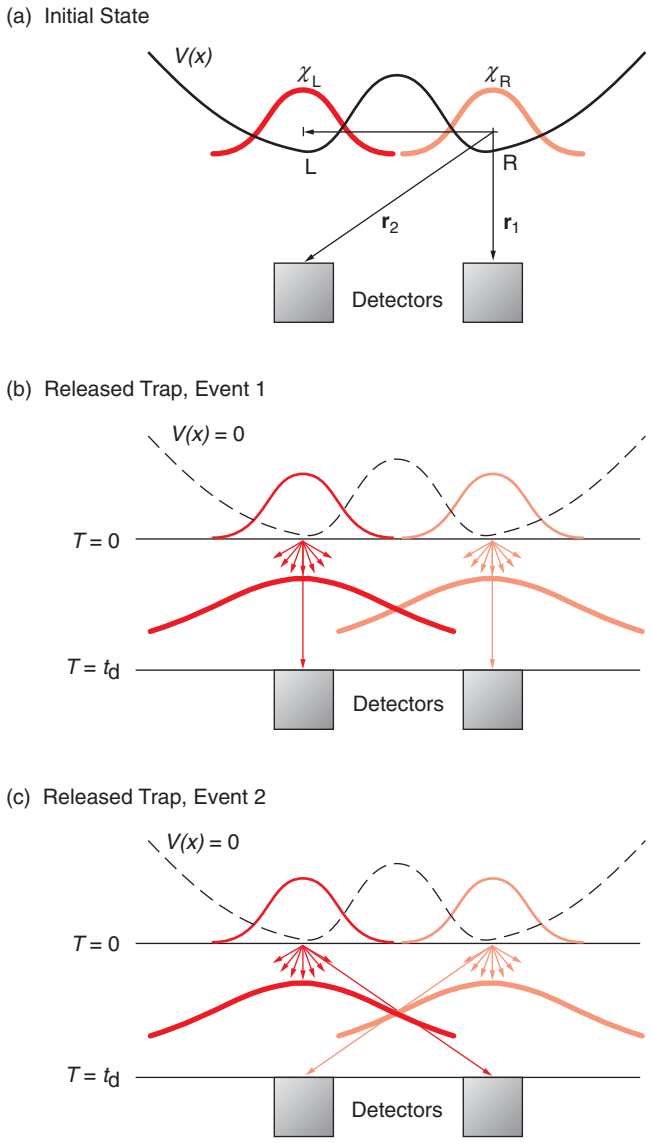

Figure 7. Origin of the Two-Particle Interference in Equation (13)
This schematic illustrates the origin of the interference pattern in the two-particle density for an expanding two-particle system that originates in a number state of a double-well potential. (a) The origin of the coordinate system is the center of the right potential well. (b) In event 1, the particle detected at $\mathbf{r}_1$ originates from the right well; the particle detected at $\mathbf{r}_2$, from the left well. (c) In event 2, the particle detected at $\mathbf{r}_1$ originates from the left well, whereas the particle detected at $\mathbf{r}_2$ originates from the right well. Because the two-particle wave function consists of a superposition of terms that correspond to the classical trajectories shown in (b) and (c), these events can interfere.

Assuming that $\mathbf{r}_1$ and $\mathbf{r}_2$ are located in the region where $|\chi_L(\mathbf{r}_1; t)| \sim |\chi_L(\mathbf{r}_2; t)| = \chi$, the two-particle density defined in Equation (12) takes on the form

$$\rho_{2(N)}(\mathbf{r}_1,\mathbf{r}_2;t) \approx \chi^4\left\{1 + \cos\left[\theta_R(\mathbf{r}_1;t) - \theta_L(\mathbf{r}_1;t) - \left(\theta_R(\mathbf{r}_2;t) - \theta_L(\mathbf{r}_2;t)\right)\right]\right\}, \quad (13)$$

which contains the typical oscillatory contribution seen in Equation (9) describing an interference pattern. Thus, although the system is in a number state and the single-particle density does not exhibit interference, the two-particle density $\rho_{2(N)}$ does show interference.

The sinusoidal contributions in Equation (13) arise from the interference of the two distinct two-particle events illustrated in Figure 7. In one event, the particle detected at $\mathbf{r}_1$ was initially in the right well, whereas the particle detected at $\mathbf{r}_2$ originated from the left well. In the second event, the situation is reversed: The particle detected at $\mathbf{r}_1$ originated from the left well, whereas the particle detected at $\mathbf{r}_2$ originated from the right well.

Using Equation (10) for the phase difference between the two single-particle wave functions at a position $\mathbf{r}$, $\theta_R(\mathbf{r}) - \theta_L(\mathbf{r}) \approx -(m/2\hbar t)[2\mathbf{d}\cdot\mathbf{r} + d^2]$, we find that the two-particle distribution depends only on the relative position $\mathbf{r}_1 - \mathbf{r}_2$,

$$\rho_{N,2}(\mathbf{r}_1,\mathbf{r}_2;t) \approx \chi^4\left\{1 + \cos\left[(m/\hbar t)\,\mathbf{d}\cdot(\mathbf{r}_1-\mathbf{r}_2)\right]\right\} . \tag{14}$$

Whereas the likelihood of detecting the first particle at position $\mathbf{r}_1$ is independent of $\mathbf{r}_1$ in the far region $\rho_{1(N)} \approx \chi^2$, the likelihood of detecting a second particle at $\mathbf{r}_2$ is greater near the planar regions $\mathbf{d}\cdot(\mathbf{r}_1 - \mathbf{r}_2) = n(ht/m)$, where n denotes an integer. Note that the planar regions of maximal $\rho_{2(N)}$-values resemble the interference fringes of $\rho_{1(C)}$ in Equation (11), namely, the single-particle density of the expanding, mutually coherent two-particle double-well system. In fact, the fringe patterns for the two-particle density will be identical to those of an equivalent mutually coherent system, provided the relative phase α is chosen so that the fringes of that equivalent system overlap the position where the first particle was detected. Because the position of the first particle is undetermined until measured, we can say that it is the act of determining the first particle's position that fixes the value of the relative phase of an equivalent mutually coherent system. The two-particle number-state probability distribution then resembles the product of one-particle probability distributions of the equivalent mutually coherent system. That equivalence is a general feature: The more particles detected in the image of an expanding number-state double-well BEC, the more the outcome of such measurement resembles that performed on a mutually coherent double-well BEC. The relative phase of the equivalent mutually coherent BEC system can be extracted from the image but cannot be determined beforehand.

The equivalence to a mutually coherent state with a value of the phase difference that is established by the act of measurement is familiar from the observation of interference of independent lasers (Pfleeger and Mandel 1967) and of the dc Josephson effect (Anderson 1986).

Relative Phase Dynamics for Two *N*-Particle BECs. Our derivation of the number-state two-particle density and its equivalence to a mutually coherent state density of undetermined relative phase is not easily generalized to a number-state double-well system with larger particle numbers. Instead, we can apply the elegant description developed for the relative phase dynamics of Josephson junctions. In this description, the dynamics between the two weakly linked superfluids is cast in terms of only two variables: α, the relative phase, and m, half the difference of the number of particles contained in each well. In fact, m and α are quantum numbers, and the number states are the eigenstates of m. We denote by $|m\rangle$ the number state of a double-well system with N-particles per well, of which $N - m$ occupy the left well and $N + m$, the right well.

An alternative set of basis functions is provided by states of good relative phase $|\alpha\rangle = N^{-1/2}\sum_m \exp(i\alpha m)|m\rangle$. The transformation from the $|m\rangle$-basis to an $|\alpha\rangle$-state representation is therefore a Fourier transform, somewhat analogous to the transformation between the traditional momentum and coordinate representations. Just as coordinates and momenta are conjugate to each other, m and α are conjugate variables. The many-body state can be expanded in either the $|\alpha\rangle$-states or the $|m\rangle$-states, $|\Psi\rangle = \int d\alpha \Psi(\alpha)|\alpha\rangle = \sum_m \Psi_m|m\rangle$, where $\Psi(\alpha)$ and Ψ_m are equivalent to the coordinate (x) and momentum (p) representations of a single-particle state. Generally, the Ψ wave function implies a spread both in the m and α variables: $\Delta m = (\langle(m - \langle m\rangle)^2\rangle)^{1/2}$, $\Delta\alpha = (\langle(\alpha - \langle\alpha\rangle)^2\rangle)^{1/2}$, where $\langle\ \rangle$ denotes the expectation value. As conjugate variables, Δm and $\Delta\alpha$ satisfy the

Heisenberg uncertainty relation $\Delta m \times \Delta\alpha \geq 1$, whereas Δx and Δp satisfy the relation $\Delta x \times \Delta p \geq \hbar$ in single-particle quantum mechanics.

To continue our comparison of BEC interference experiments with single-particle quantum mechanics, we note that the establishment of a relative phase between interfering BECs is the analogue of a position measurement on a particle in a plane-wave state. When the plane wave has a well-defined momentum, then $\Delta p = 0$ and $\Delta x \rightarrow \infty$. The latter expression means that the coordinate has maximum uncertainty, and therefore, a measurement of x could yield any value. Likewise, in the initial state of the interfering BEC experiment, $\Delta m = 0$, and the determination of α achieved by the imaging of the expanding BECs could yield any value. When the measurement is performed, however, the wave function collapses to an eigenstate of α.

Squeezing the Numbers in BECs—Macroscopic Quantum Fluctuations

As mentioned previously, the number-phase description in terms of the α or m quantum eigenvalues is familiar from the treatment of Josephson junctions. The application of the number-phase description to the problem of double-well BECs then reveals an intimate connection between the physics of BEC interference and Josephson physics. However, the BEC interference experiment conducted at MIT lacks the weak link through which the superfluids can exchange their boson particles. Consequently, it is not exactly a BEC-Josephson experiment. In a subsequent effort, the Kasevitch group at Yale used a related setup and succeeded in inducing and controlling such reversible superflow between multiple BECs. The Yale experimentalists achieved this goal by trapping the BECs in the potential minima of an optical lattice—a trapping potential that oscillates sinusoidally in space as $|E_0|^2 \sin^2(kx)$—and by lowering and raising the potential barriers separating the BECs through variations of $|E_0|^2$. Most important, the Yale group probed Josephson physics by observing variations in the interference pattern of the expanding BECs after switching off the optical-lattice potential. The sharpness of the interference fringes revealed the uncertainty in relative phase, $\Delta\alpha$, of the expanding BECs. In particular, when the barrier height had been sufficiently increased before the BECs were released, the fringes observed in the image of the expanding BECs became fuzzy, an indication that the uncertainty in the phase values of the initial BECs had increased markedly. This increase is expected as the number uncertainty decreases. As we argue below, this is a genuine quantum fluctuation effect observed in a macroscopic system. To set the stage, we start by elucidating the role of the quantum fluctuations in multiple-well BEC physics.

Quantum and Classical Physics of Double-Well BECs. As in Equation (1), the classical or mean-field description of the N-particle double-well system, the many-body wave function is a product state: $\Psi(\mathbf{r}_1, \mathbf{r}_2, \ldots, \mathbf{r}_N;t) \approx \chi(\mathbf{r}_1;t)\ldots, \chi(\mathbf{r}_N;t)$, where each single-particle wave function is a linear superposition of left-well (χ_L) and right-well (χ_R) wave functions,

$$\chi(\mathbf{r};t) = 1/(2N)^{1/2}[(N - m(t))^{1/2}\chi_L + e^{i\alpha}(N + m(t))^{1/2}\chi_R] \ , \qquad (15)$$

and α and m are well-defined parameters. We use the same notation as in the number-phase description because the physical interpretation of α and m is the same as that of the quantum eigenvalues introduced above. In fact, $\alpha(t)$ and $m(t)$ in Equation (15) are the expectation values of the quantum treatment of the number-phase dynamics. The classical treatment can then describe superfluid effects, the essence of which relies on

Figure 8. The Bose-Hubbard Model
The diagram shows an optical-lattice potential occupied by atoms of integer spin. The interactions between the atoms include a hopping or tunneling interaction and a repulsive interaction between atoms at the same site.

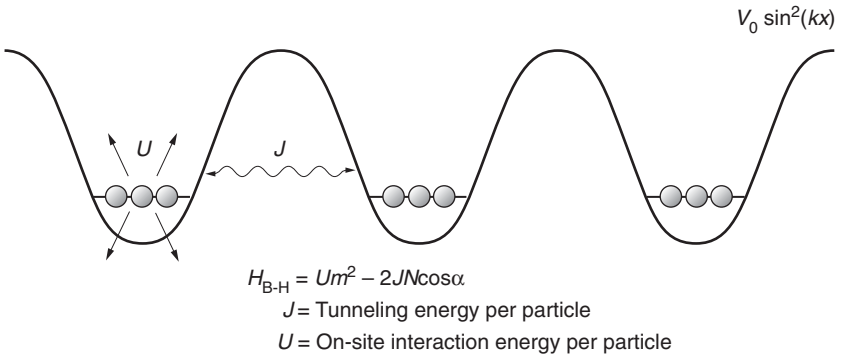

the existence of a well-defined phase—see Equations (1) to (4) and the section "The Coherent Wave Nature of Superfluidity"—but it cannot account for behavior such as the collapse to a random value of the relative phase in the imaging of interfering BECs. More generally, contrary to predictions of classical mechanics, the quantum treatment predicts different outcomes of identical measurements on identically prepared systems. Measures of such quantum randomness are the standard deviations, such as the deviations $\Delta\alpha$ and Δm introduced earlier, that quantify the range of quantum fluctuations. For sufficiently large numbers of atoms, Δm can take on values that are large enough for the fluctuation range to be called "macroscopic."

Weakly Linked BECs. When the barrier separating the two potential wells in the double-well BEC is lowered to an appropriate value, atoms can penetrate the barrier, which thereby provides the weak link that allows the left and right BECs to exchange particles. As in the description of BEC interference, we define a phase for each BEC and describe the possible particle exchange in terms of the canonically conjugate variables that represent the difference of the condensate phases, α, and half the difference of the particle population, m, occupying the individual BECs. The inter-BEC particle exchange gives rise to an effective tunneling energy of the usual Josephson form,

$$E_{\text{tun}} = -E_J \cos(\alpha) \ . \tag{16}$$

We expect the value of E_J to be roughly proportional to the number of particles (N) per well, to depend weakly on the number difference m, and to be extremely sensitive to the height of the potential barrier separating the BECs. As the barrier height increases, the tunneling of particles is restricted, a limitation corresponding to a decrease in the value of the E_J-parameter in Equation (16). In what follows, we write $E_J = 2NJ$, where J denotes the tunneling energy per particle. The tunneling energy, minimized by putting $\alpha = 0$, favors a well-defined value of the phase difference in the ground state and, hence, favors the establishment of a definite phase difference (the superfluid limit). In contrast, the usual interparticle interactions, if repulsive, favor a well-defined value of m. To see that, we note that the interparticle interaction energy scales as the number of interactions. The N_L-particles (in the left BEC) experience $N_L(N_L - 1)/2 \approx N_L^2/2$ interactions. Similarly, the N_R-particles (contained in the right well) undergo $N_R^2/2$ interactions. Assuming that the interaction energy per particle, U, is approximately the same in each well and using $N_L = N - m$ and $N_R = N + m$, we write the total interaction energy as

$$E_{\text{int}} = (U/2)\left[N_{\text{R}}^2 + N_{\text{L}}^2\right] \approx U\left[N^2 + m^2\right] . \quad (17)$$

In contrast to the tunneling energy, E_{int} takes on its minimum value at $m = 0$, corresponding to the BEC number state with $N_{\text{R}} = N_{\text{L}} = N$. The contribution to the energy that stems from the phase-number dynamics (the sum of interaction and tunneling energies after the constant UN^2-term has been discarded) is then equal to

$$H = Um^2 - 2JN\cos(\alpha) . \quad (18)$$

Classically, the position of lowest energy is $m = 0$, $\alpha = 0$. Quantum mechanically, it follows from Heisenberg's uncertainty principle that m and α, being conjugate variables, cannot be determined simultaneously to absolute certainty. We now use the double-well Bose-Hubbard Hamiltonian in Equation (18) as a starting point to indicate how weakly linked BECs can be regarded as a laboratory for exploring both the classical dynamics and the quantum nature of Josephson junctions. A schematic representation of the individual terms that contribute to this Hamiltonian is shown in Figure 8.

Probing Josephson Physics in Weakly Linked BECs. The Bose-Hubbard Hamiltonian in Equation (18) is the generic form of the Hamiltonian that governs the physics of Josephson junctions. We can expect, therefore, that the atom trap becomes a new laboratory for studying Josephson effects. Although this physics has been studied intensely in condensed-matter environments, the new parameter range and technology of the BEC traps give a new twist to the study of Josephson-junction physics and other known phenomena, as well as the opportunity to study quantum fluctuations and, perhaps, to discover novel applications.

A sudden change in the depth of one of the wells or in its particle number can "nudge" the many-body system out of equilibrium, initiating a collective excitation in which the expectation value of the well populations oscillates. This phenomenon is called Josephson oscillations. On the topic of probing quantum behavior, it is interesting that the parameters in Equation (18) can be controlled experimentally: Variations in the trapping potential can alter the values of U and J. Clearly, the atom-trap technology gives unusual control over the Josephson junction, providing new knobs that can both initiate Josephson oscillations and vary the quantum fluctuations. The crucial question of whether oscillations and fluctuations can be measured in cold-atom BECs was answered, in part, by the Yale experiment.

What are the obstacles that the BEC technology faced in probing Josephson physics? In superconductors, Josephson effects are routinely studied by measurements of the weak supercurrent. Such measurement of a charged particle can be achieved relatively simply and accurately. In systems of neutral particles, on the other hand, the observation of a weak current represents a much greater challenge, and in helium fluids, a Josephson current was only recently observed (Packard 1998). By the same token, in the neutral-atom traps, current atom-counting techniques are not sufficiently accurate to allow observing small-amplitude population oscillations. Numbers of atoms in a typical BEC are measured with a relative accuracy of only about 10 percent. This low accuracy renders the technique unsuitable for observing Josephson oscillations of atomic-trap populations in the linear regime (number oscillations with a magnitude of 1 percent or less of the total number of trapped atoms). Instead of measuring a population imbalance,

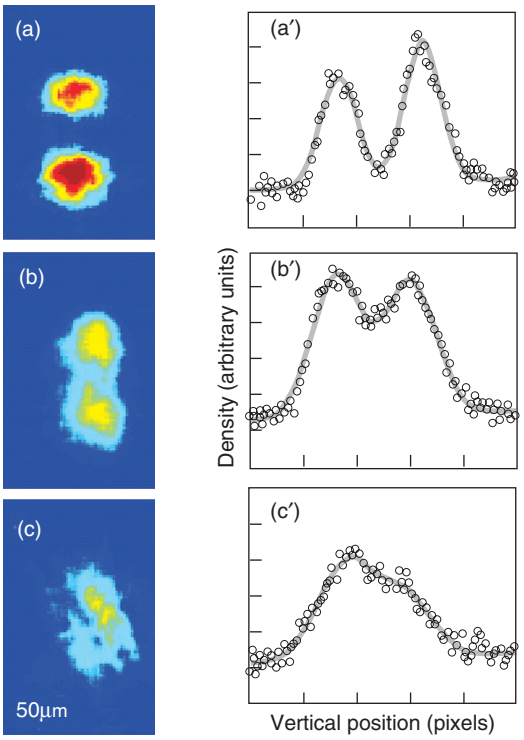

Figure 9. Formation of Number-Squeezed States in an Atom-Trap BEC
The sequence of absorption images, (a)–(c), and the associated density cross sections, (a′)–(c′), show atoms released from optical lattices of increasing depth: $U_0 = 7.2E_{recoil}$, $U_0 = 18E_{recoil}$, and $U_0 = 44E_{recoil}$, respectively. In (a), the two-peaked structure is due to interference between atoms released from different lattice sites. As the well depth increases and the tunneling rate decreases, the interference pattern becomes progressively blurred, reflecting greater phase uncertainty and the formation of number-squeezed states.
(Reprinted with permission from Orzel et al. *Science* 291, page 2389. Copyright 2001 American Association for the Advancement of Science.)

we might try to observe the relative phase of BECs, which gives a complementary view of the physics; for instance, the expectation value of the relative phase oscillates at the same frequency as the population imbalance or current in the Josephson oscillation. The BEC interference experiment conducted at MIT illustrated that the relative phase can be measured from recorded images of expanding BECs. This measurement, however, is destructive and yields a value for the phase at a single time. Whether this technique could be used to probe the time evolution of the phase is not evident. In addition, the imaging of BEC interference in the double-well system gives only a single value of the phase, whereas a measurement of the range of quantum fluctuations requires a record of the phase distribution.

The Yale experiment resolved the problem of probing the phase distribution by imaging the interference of many simultaneously expanding BECs, which had been weakly linked before the trapping potential was released. The resulting image is sensitive to the distribution of the complex phase values of the BECs. If the phases of the BECs are strongly correlated—they all have approximately the same value, for instance—then the interference of each pair of BECs can add up in phase and give an overall pattern with bright and sharp fringes. In contrast, if the phases of the weakly linked BECs are randomly distributed, then their values, determined by the act of imaging, differ widely. As a consequence, the fringes corresponding to the interference of different pairs of BECs do not overlap, so that interference washes out. The Yale experiment imaged the density of 12 expanding BECs that had been initially trapped in the adjacent potential wells of a linear optical lattice and weakly linked before the optical-lattice potential was released (see Figure 9). In such an optical lattice, the centers of mass of adjacent BECs are all separated by the same distance (half the wavelength of the light that creates the standing wave pattern of the lattice potential). By measuring the amplitude and fringe sharpness (defined as the ratio of spatial width to the distance separating the fringes) observed in imaging the expanding BECs, the Yale group quantified the uncertainty of the relative phase values.

As they had ramped up the height of the potential barriers before releasing the BECs, the Yale group observed a marked decrease in the sharpness of the fringes in the expanding-BEC images. The measured sharpness was in quantitative agreement with numerical simulations that were based on the ground-state phase uncertainty. The assumption that the many-body system has reached its ground state before the trapping potentials are switched off is reasonable because the change in potential barrier was effected adiabatically in the experiments. In a ground state, the uncertainties of conjugate variables generally reach the Heisenberg limit, which in this case would mean that $\Delta m \times \Delta\alpha \approx 1$. Thus, from their measurements and the agreement with the predicted values of phase uncertainty, the Yale group inferred that their observed

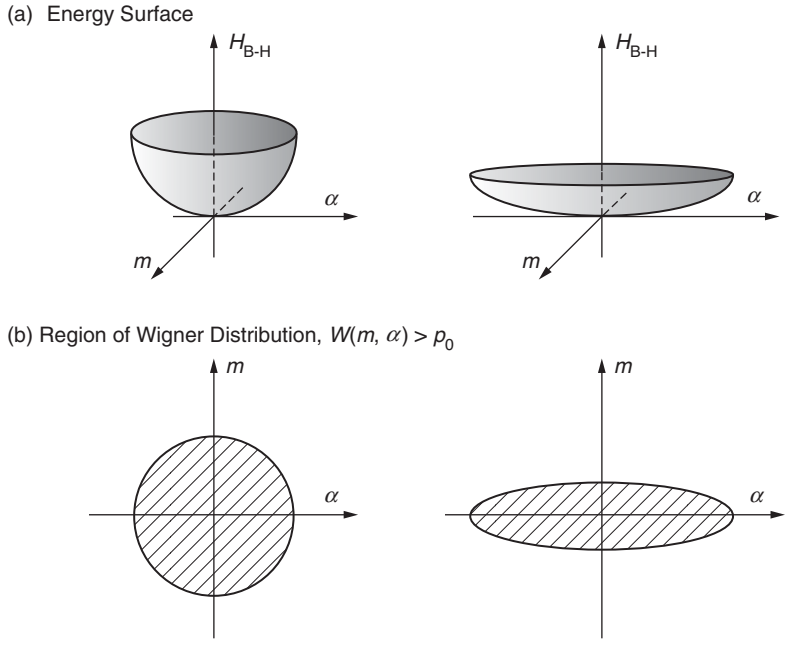

Figure 10. Number Squeezing in Phase Space
This graph illustrates the physics of number squeezing by showing the effect of an increase in the potential barrier on the number phase (m, α) Wigner distribution of the double-well BEC discussed in the text. The graphs show the area in which the Wigner distribution of the many-body ground state exceeds a minimal value. An increase in the potential barrier lowers the tunneling rate J, which reduces the {tightness of confinement in the α-direction of the (m, α) phase space. The word "confinement" refers to the potential energy-like term in the energy expression of Equation (18) that depends on α. As a result of lowering J, the ground-state Wigner distribution stretches out in the α-direction. In accordance with the Heisenberg uncertainty principle ($\Delta m \Delta\alpha \approx 1$), the area of high Wigner distribution value remains constant in the process of stretching and the number uncertainty Δm decreases accordingly.

increase in phase uncertainty implied a similar decrease in number uncertainty Δm. By analogy with a similar reduction of uncertainty in optical field intensities, the process of reducing $\Delta m << N^{1/2}$ is called "squeezing." In Figure 10, we further illustrate the aptness of this term by sketching the effect of varying the parameters of the Hamiltonian in Equation (18) on the Wigner distribution function.

The experimental increase of the potential barrier height lowers the value of J, which greatly reduces the tightness of the confinement in the α-direction of the (α, m)-phase space. In response, the Wigner distribution stretches out farther in the α-direction. Since the area of high probability shown in Figure 10 remains of order 1, the uncertainty in the m-direction is tightly squeezed. Thus, as the hopping motion of particles between adjacent wells is "frozen out," each well contains a better-defined number of particles. To further support their claim of having observed quantum fluctuations, the Yale group also demonstrated that the trend of decreased fringe sharpness may be turned around by reversal of the variation in potential barrier height.

Quantitative Treatment of Number Squeezing. We now revisit the description of the double-well BEC to provide a quantitative understanding of the number uncertainty squeezing illustrated in Figure 10. We introduce a dimensionless parameter, or coupling constant Γ, that characterizes the competing interactions in the system: $\Gamma = UN/2J$ is the ratio of the interparticle interaction energy per well ($UN^2/2$) to the tunneling energy per well NJ (the latter plays a role somewhat analogous to that of kinetic energy in other systems). We minimize the Hamiltonian described by Equation (18) in the α-representation. To convert Equation (18) from the number representation to the α-representation, we replace the m-operator by $-(1/i)\partial/\partial\alpha$. Then, we calculate the expectation value of the Hamiltonian by using the Gaussian state for the wave function ψ, $\psi(\alpha) \propto \exp(-\alpha^2/(4x))$. The expectation values are simplified when expressed in terms of the width parameter x, which is related to the uncertainty in phase difference as $\Delta\alpha = (2x)^{1/2}$: $\langle m^2 \rangle = -\langle \partial^2/\partial\alpha^2 \rangle = 1/(2x)$ and $\langle \cos(\alpha) \rangle = \exp(-x)$.

The expectation value of the Hamiltonian is then equal to

$$\langle H \rangle = \frac{U}{2}\left[\frac{1}{x} - \frac{2N^2}{\Gamma}\exp(-x)\right] \tag{19}$$

and we obtain the value of the width parameter x by minimizing Equation (19):

$$x = \sqrt{\frac{\Gamma}{2N^2}}\exp(x/2) \ . \tag{20}$$

In the weakly coupled regime $\Gamma << 2N^2$, the minimum expectation value occurs at a value $x << 1$, in which case $\exp(x/2) \approx 1$ and Equation (20) yields the width parameter $x \approx (\Gamma/2)^{1/2}/N$. In other words, the weakly coupled case yields a very small phase uncertainty,

$$\Delta\alpha = (2x)^{1/2} \approx (2\Gamma)^{1/4}/N^{1/2} << 1 \ , \tag{21}$$

and therefore corresponds to the superfluid limit. Most superconducting Josephson junctions find themselves in this limit. Because the number uncertainty is small, $\Delta\alpha \sim N^{-1/2}$, the classical (or mean-field) approximation successfully describes these Josephson experiments. The uncertainty in particle number $\Delta m \approx N^{1/2}/2\Gamma^{1/4}$ appears Poissonian ($\Delta N \approx N^{1/2}$) if we write it in terms of the coupling constant. The small phase uncertainty in this regime is not easily measured with appreciable accuracy.

In contrast, as the value of J is lowered by an increasing barrier height, the coupling constant $\Gamma = [UN/2J]$ increases accordingly, and the phase uncertainty can increase to give a measurable decrease in fringe sharpness. In the Yale experiment, the increase in the potential barrier was sufficient to allow the system to approach the strong coupling regime $\Gamma \sim N^2$ or $U/J \sim N$. In that regime, the value of x at the minimum energy can become of order 1, in which case we cannot replace $\exp(x/2)$ by 1. Instead, we must solve Equation (20). By the time the potential barrier has been increased to the point that, say, $U/J = (4/e)N$, the variation becomes $\Delta m = (\mathrm{l}/2)^{1/2}$, and the uncertainty in atomic population of each well has dwindled to less than one particle. At that point, $\Delta m << N^{1/2}$, and we say that the number distribution has become sub-Poissonian. The phase-difference uncertainty, $\Delta\alpha$, also becomes of order unity. Well before that point, say, when U/J is increased to only 10 percent of N, or $U/J = 0.1N$, the uncertainty in phase difference in the double-well BEC has grown to half a radian. In the multiple-well BEC system, the uncertainty in phase between nonadjacent wells under that same condition, $U/J = 0.1N$, is greater, and the loss of fringe sharpness in the interference of 12 BECs is quite noticeable.

From Superfluid to Mott Insulator

By illustrating number squeezing, the Yale group demonstrated that BEC technology can engineer and observe quantum fluctuations of an almost macroscopic system. On the other hand, technical constraints in the Yale experiment limited the height to which the potential barrier could be raised and, hence, the range to which the number uncertainty could be squeezed. These limitations prevented the Yale group from venturing further into the strong-coupling regime. By pushing this frontier, Hänsch's group in Munich were able to observe a very interesting phase transition (Figures 11 and 12). As they squeezed the number uncertainty below a value of order 1—it would be $(1/2)^{1/2}$

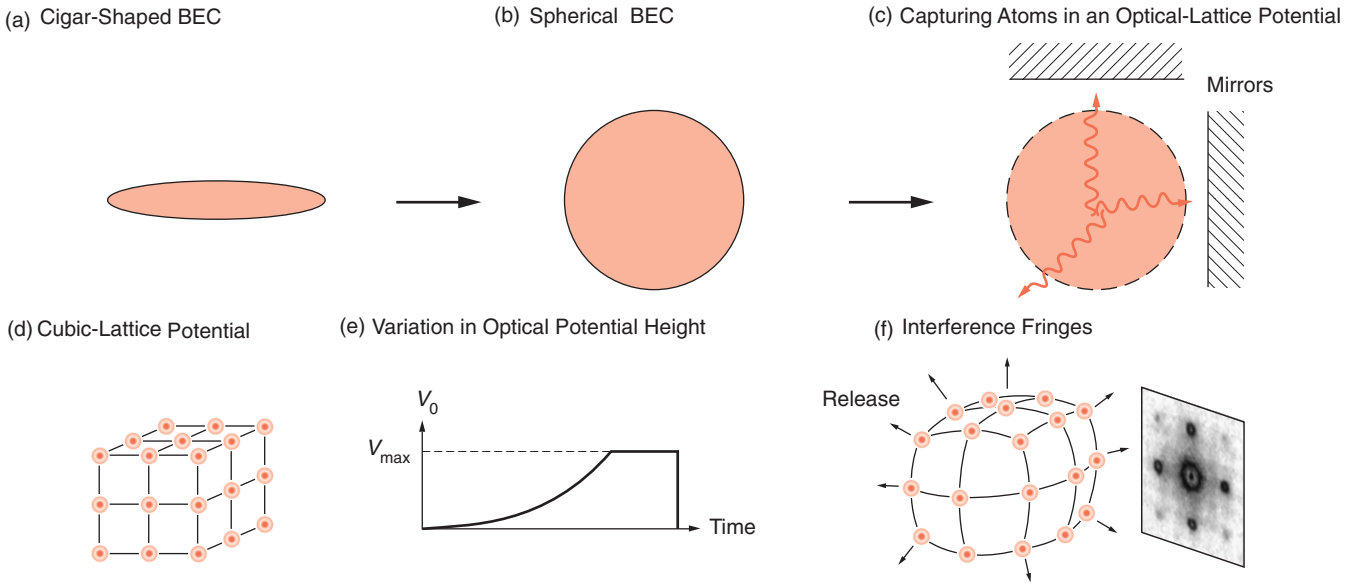

Figure 11. Demonstration of a Transition from a Superfluid to a Mott Insulator

In the BEC experiment that demonstrated the quantum phase transition from a superfluid to a Mott insulator (Greiner 2002), the experimentalists started with a cigar-shaped BEC (a) that was relaxed to a spherical BEC (b), distributing the atoms more evenly over a larger region of space. By shining in three laser beams, detuned from each other and reflected by mirrors, the researchers created a standing-wave pattern that captures the atoms in an optical-lattice potential (c): $V(x, y, z) = V_0[\sin^2(kx) + \sin^2(ky) + \sin^2(kz)]$, where k denotes the wave vector of the laser light. Gradual increases in laser intensity and, hence, in the potential V_0 trap one to three atoms per potential minimum, or well. These minima form a cubic lattice (d). In (e) we show a typical variation of the optical potential height V_0: The potential height is ramped up "slowly" for 80 ms and kept constant for another 20 ms; then the trapping potential is suddenly switched off, at which point the atoms in the BEC begin to expand. In (f), the atomic wave functions from different wells begin to overlap, and the atomic density imaged in a plane shows interference fringes.

in the approximations introduced previously—the ground state abruptly changes to a Fock or number state with $\Delta m = 0$. This phenomenon is a true phase transition: Many-body properties change suddenly as $U/J \sim N$. In addition to the change in number statistics, the system's conductivity alters discontinuously as the system takes on a number state. In the number state, a finite amount of energy is required to transfer atoms between wells; therefore, the transition to the number state abruptly alters the nature of the many-body system from a conductor with superfluid properties to a Mott insulator. This many-body phenomenon is an example of a transition driven by the competition between different interactions, rather than by the competition between order and disorder, which is responsible for usual phase transitions. If they involve quantum fluctuations, the former transitions (which occur at zero temperature) are called quantum phase transitions.

If we can trust the tunneling energy in Equation (16) and the interaction energy in Equation (17) to accurately describe the many-body physics, then the BEC in an optical lattice is an example of a Bose-Hubbard system. The theory of the phase transition from superfluid to Mott insulator in such systems has been explored in great detail. Experimentally, this transition was first observed in an array of superconducting Josephson junctions. In BEC physics, the experimental study of the transition by the Munich group demonstrated, once again, that the BEC technology gives an unusual degree of control.

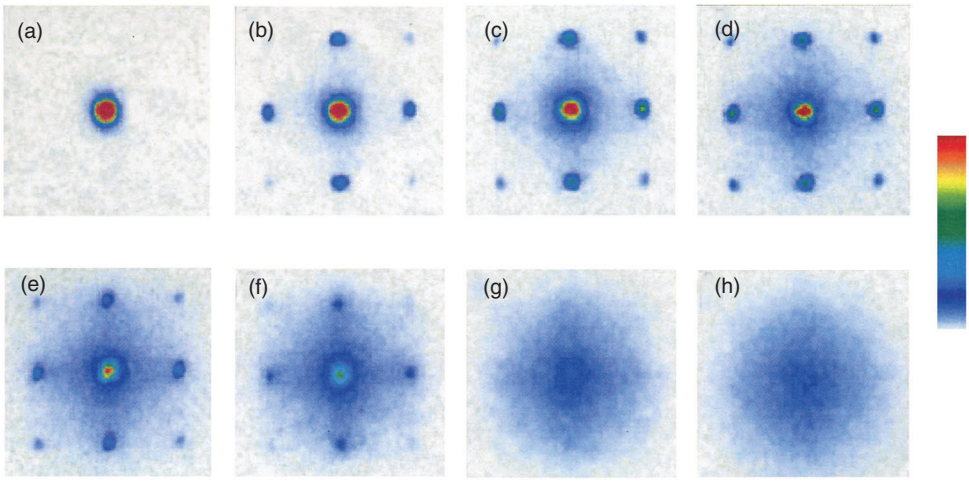

Figure 12. Absorption Images Showing a Transition to a Mott Insulator in a BEC
The BEC absorption images (a)–(h) were recorded in a particular plane 15 ms after the trapping potential was switched off. The images reflect different maximum values V_{max} of V_0. In units of the recoil energy, $E_{recoil} = \hbar^2k^2/2m$ (capital R was used for "right"), V_{max} took on the values (a) 0, (b) $3E_{recoil}$, (c) $7E_{recoil}$, (d) $10E_{recoil}$, (e) $13E_{recoil}$, (f) $14E_{recoil}$, (g) $16E_{recoil}$, and (h) $20E_{recoil}$. Notice that the interference pattern completely disappears between $V_0 = 14E_{recoil}$ and $V_0 = 16E_{recoil}$, in agreement with the prediction that all phase information would be lost as the potential barriers increase and the atoms become localized in their respective potential wells.
(This figure was reproduced courtesy of *Nature*.)

Before describing the experiment, we demonstrate the transition in the double-well BEC system. From Equation (19), we see that, in the limit of large phase uncertainty ($x \to \infty$), the expectation value of the number-phase energy—Equation (18)—vanishes. Consequently, when the local minimum of $\langle H \rangle$ takes on a positive value, the true minimum of the system is found at $x \to \infty$, as we illustrate in Figure 13. As the value of U/JN increases, the value of the local minimum increases until, at $U/J = (4/e)N$, corresponding to $\Delta\alpha = 2^{1/2}$ and $\Delta m = 2^{-1/2}$, the value of the minimum turns positive and the real minimum is at $x \to \infty$, corresponding to $\Delta\alpha \to \infty$ and $\Delta m = 0$.

A significant difference between the Yale and Munich experiments lies in the number of potential wells created in the optical lattices. The trapping potential in Hänsch's group was a three-dimensional lattice of 65 sites in each dimension. The large number of lattice sites in the Munich experiment, 65^3 in total, is significant because it allows experimentalists to trap one to three particles per site while still having a sufficiently large total number of atoms to image the interference of the expanding BECs. By lowering the value of N (N was about 10,000 in the Yale experiment), the Munich group could reach the critical ratio of $U/J \sim N$ with a much smaller increase in barrier height. Actually, the simple (α, m) treatment of the number-phase dynamics in the double-well BEC becomes invalid for small values of N and a different description, such as the one presented by Subir Sachdev (1999), is necessary. Nevertheless, the (α, m) description still captures the main features and predicts the correct order of magnitude of the transition point. Hänsch's group also probed the excitations of this system and found evidence for the insulator property of a finite energy (or "gap") necessary to allow transferring atoms between wells. Again, these experiments illustrate the unprecedented tools offered by the cold-atom technology.

Los Alamos Achievements and Future Work

With regard to fundamental physics, we have shown that BEC experiments can probe beyond the confines of traditional condensed-matter Josephson-junction studies by exploring and engineering quantum fluctuations. We have also emphasized that atom-laser systems with superfluid properties (long-range phase coherence in an equilibrium as opposed to a nonequilibrium state) may offer unique opportunities for application. For instance, the BECs may find novel uses in atom interferometry and sensing applications.

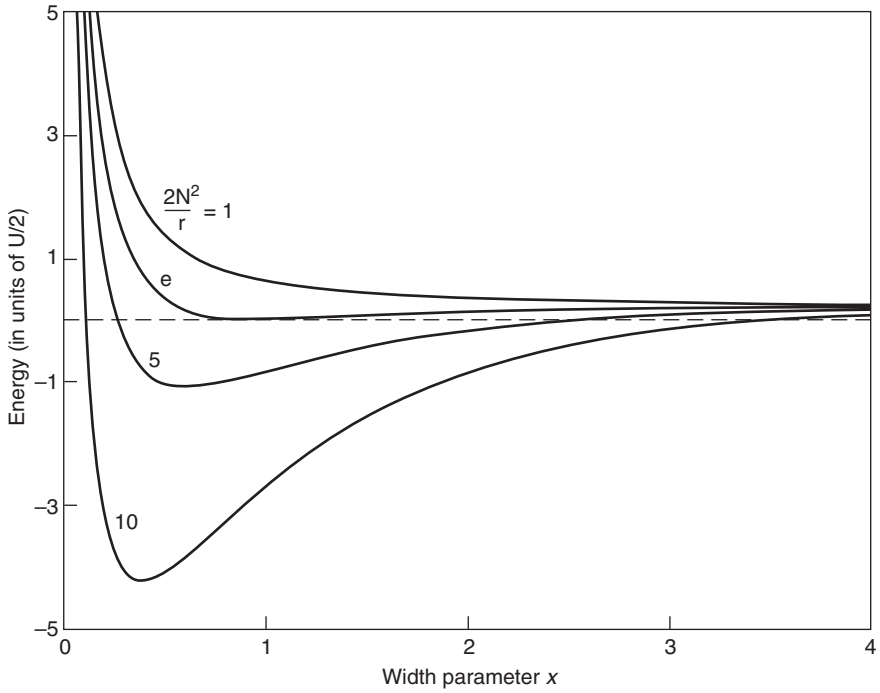

Figure 13. Number-Phase Energy for Different Interaction Parameters
The expectation values of the number-phase energy of Equation (18) are calculated with a Gaussian trial wave function $\psi(\alpha) \propto \exp(-\alpha^2/[4x])$ and are plotted as a function of the width parameter *x*, which is related to the phase uncertainty $\Delta\alpha$ as $x = (\Delta\alpha)^2/2$. The different curves show $H(x)$ for different values of the interaction parameter $(2N^2/\Gamma)$. From bottom to top, those values are 10, 5, *e*, and 1. For $(2N^2/\Gamma) < e$, the local minimum is also the global minimum, whereas for $(2N^2/\Gamma) > e$, the global minimum occurs in the limit $x \to \infty$, corresponding to a complete uncertainty of the phase.

Hopefully, this historical perspective has also conveyed a sense of the flexibility of the cold-atom-trap technology. That flexibility has led to a host of other avenues being pursued or contemplated: for instance, schemes to alter and control the nature and strength of the interparticle interactions, already successful searches for superfluid properties in BECs, demonstrations of nonlinear physics effects in superfluids (vortices, solitons, and "quantum shocks"), the study of mutually coherent BECs, the demonstration of atom-molecule BECs, and the prospect of using BECs for the study of quantum measurement theory.

Los Alamos National Laboratory has been active in exploring several of the above aspects. The following are some of the Los Alamos contributions and ongoing projects that we are aware of. On the experimental side, David Vieira and Xinxin Zhao are working toward the use of an atomic BEC to cool down fermion atoms (see the article "Experiments with Cold Trapped Atoms" on page 168). On the theoretical side, Peter Milonni was the first to point out that external electric fields can be used to control the interparticle interactions in the atom-trap systems (Milonni 1996). Diego Dalvit, Jacek Dziarmaga, and Wojciech Zurek resolved the puzzle of the lifetime of the proposed Schrödinger cat states in BEC-like systems, and they have proposed schemes to reduce the effect of decoherence and increase the cat's longevity (see the article "Schrödinger Cats in Atom-Trap BECs" on page 166). In collaboration with experimentalist Roberto Onofrio (visiting from the University of Padua, Italy), they continue to explore the possible use of BECs in studies of measurement theory. Lee Collins has explored the vortex and soliton dynamics in BECs, working closely with the experimental group of Bill Philips at the National Institute of Standards and Technology (Denschlag et al. 2000). Gennady Berman and Augusto Smerzi are exploring the possibility of using BECs to study the boundary between quantum and classical behavior (Berman et al. 2002), as well as using BECs in optical lattices for interferometry purposes (Dziarmaga et al. 2002).

Since 1996, I have also been active in BEC research. The prediction for the phase separation of BECs under specific conditions (Timmermans 1998) has been confirmed by experiments in Ketterle's group at MIT. This same group also confirmed our

predictions for the reduction of scattering slow distinguishable particles by the BEC (Timmermans and Côté 1998) and for the excitation rate of phonon modes in two-photon scattering experiments. Recently, the group of Wieman at JILA found evidence for a prediction by Timmermans et al. (1999) of the formation of an atom-molecule BEC in the Feshbach resonance scheme that was initially proposed to alter the effective interparticle interactions. In a recent collaboration with Milonni of Los Alamos and Arthur Kerman of MIT, I pointed out the possibility of creating a fermi-on-boson superfluid (Timmermans et al. 2001) by bringing an ultracold fermion gas mixture near a Feshbach resonance. Finally, I discovered the heating mechanism that explains the temperature limit encountered by efforts in fermion atom cooling and provides the main obstacle for the current experiments to reach fermion superfluidity in atom traps (Timmermans 2001a).

The variety of approaches and cold-atom research topics at Los Alamos is yet another measure of the richness of this field. By now, numerous experiments have established the cold-atom trap as a new kind of laboratory in which to study interesting fundamental issues in low-temperature, many-body, and nonlinear physics. The unusual control and the variety of experimental knobs also hint at the possibility of practical applications. Hopefully, Los Alamos can continue to play a significant role in the ongoing cold-atom physics adventure. ■

Further Reading

Anderson, P. W. 1986. Measurement in Quantum Theory and the Problem of Complex Systems. In *The Lesson of Quantum Theory*. p. 23. Edited by J. D. Boer, E. Dal, and O. Ulfbeck. Amsterdam: Elsevier.

Anderson, M. H., J. R. Ensher, M. R. Matthews, C. E. Wieman, and E. A. Cornell. 1995. Observation of Bose-Einstein Condensation in a Dilute Atomic Vapor. *Science* **269**: 198.

Andrews, M. R., C. G. Townsend, H. J. Miesner, D. S. Durfee, D. M. Kurn, and W. Ketterle. 1997. Observation of Interference between Two Bose Condensates. *Science* **275**: 637.

Berman, G. P., A. Smerzi, and A. R. Bishop. 2002. Quantum Instability of a Bose-Einstein Condensate with Attractive Interaction. *Phys. Rev. Lett.* **88**: 120402.

Bradley, C. C., C. A. Sackett, J. J. Tollett, and R. G. Hulet. 1995. Evidence of Bose-Einstein Condensation in an Atomic Gas with Attractive Interactions. *Phys. Rev. Lett.* **75**: 1687.

Davis, K. B., M.-O. Mewes, M. R. Andrews, N. J. van Druten, D. S. Durfee, D. M. Kurn, and W. Ketterle. 1995. Bose-Einstein Condensation in a Gas of Sodium Atoms. *Phys. Rev. Lett.* **75**: 3969.

Denschlag, J., J. E. Simsarian, D. L. Feder, C. W. Clark, L. A. Collins, and J. Cubizolles. 2000. Generating Solitons by Phase Engineering of a Bose-Einstein Condensate. *Science* **287**: 97.

Dziarmaga, J., A. Smerzi, W. H. Zurek, and A. R. Bishop. 2002. Dynamics of Quantum Phase Transition in an Array of Josephson Junctions. *Phys. Rev. Lett.* **88**: 7001.

Greiner, M., O. Mandel, T. Esslinger, T. W. Hänsch. and I. Bloch. 2002. Quantum Phase Transition from a Superfluid to a Mott Insulator in a Gas of Ultracold Atoms. *Nature* **415**: 39.

Huang, K. 1987. *Statistical Mechanics*. Second Edition. New York: John Wiley & Sons.

London, F. 1938. The λ-Phenomenon of Liquid Helium and the Bose-Einstein Degeneracy. *Nature* **141**: 643.

Madison, K. W., F. Chevy, W. Wohlleben, and J. Dalibard. 2000. Vortex Formation in a Stirred Bose-Einstein Condensate. *Phys. Rev. Lett.* **84**: 806.

Milonni, P. W., and A. Smith. 1996. van der Waals Dispersion Forces in Electromagnetic Fields. *Phys. Rev. A* **53**: 3484.

Orzel, C., A. K. Tuchman, M. L. Fenselau, M. Yasuda, and M. A. Kasevitch. 2001. Squeezed States in a Bose-Einstein Condensate. *Science* **291**: 2386.

Packard, R. E. 1998. The Role of the Josephson-Anderson Equation in Superfluid Helium. *Rev. Mod. Phys.* **70**: 641.

Pais, A. 1979. Einstein and the Quantum Theory. *Rev. Mod. Phys.* **51**: 861.

Penrose, O. 1951. On the Quantum Mechanics of Helium II. *Philos. Mag.* **42**: 1373.

Penrose, O., and L. Onsager. 1956. Bose-Einstein Condensation and Liquid Helium. *Phys. Rev.* **104**: 576.

Pfleegor, R. L., and L. Mandel. 1967. Interference of Independent Photon Beams. *Phys. Rev.* **159**: 1084.

Rayfield, G. W., and F. Reif. 1964. Quantized Vortex Rings in Superfluid Helium. *Phys. Rev.* **136**: A1194.

Sachdev, S. 1999. Chapter 10 in *Quantum Phase Transitions*. Cambridge: Cambridge University Press.

Timmermans, E. 1998. Phase Separation of Bose-Einstein Condensates. *Phys. Rev. Lett.* **81**: 5718.

———. 2001a. Degenerate Fermion Gas Heating by Hole Creation. *Phys. Rev. Lett.* **87**: 240403.

———. 2001b. Superfluids and Superfluid Mixtures in Atom Traps. *Contemp. Phys.* **42**: 1.

Timmermans, E., and R. Côté. 1998. Superfluidity in Sympathetic Cooling with Atomic Bose-Einstein Condensates. *Phys. Rev. Lett.* **80**: 3419.

Timmermans, E., K. Furuya, P. W. Milonni, and A. K. Kerman. 2001. Prospect of Creating a Composite Fermi-Bose Superfluid. *Phys. Lett. A* **285**: 228.

Timmermans, E., P. Tommasini, R. Côté, M. Hussein, and A. Kerman. 1999. Rarified Liquid Properties of Hybrid Atomic-Molecular Bose-Einstein Condensates. *Phys. Rev. Lett.* **83** (14): 2691.

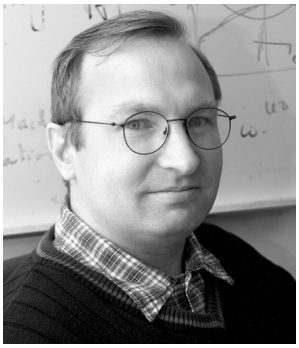

Eddy Timmermans is currently an Oppenheimer postdoctoral fellow at Los Alamos National Laboratory and will soon join the permanent staff of the Theoretical Division. He received his Ph.D. in condensed-matter theory from Rice University (1995) and then became a fellow at the Harvard-Smithsonian Institute for Theoretical Atomic and Molecular Physics (1995–1998). There, he became interested in the physics of ultracold-atom systems. His most recent research has explored issues of and prospects for fermion pairing in ultracold-atom systems.